

Figure 2—Adipocyte-specific *Enpp2* KO mice showed smaller weight gains when fed a high-fat diet. *Enpp2*^{F/F} *Fabp4*-Cre (Fat-*Enpp2* KO) mice were generated and compared with control *Enpp2*^{F/F} littermates of the same generation (shown as WT). Fat-*Enpp2* KO and WT mice were fed either an ND or a high-fat diet (DIO) for 10 weeks. All mice were examined when they were 17 weeks old. **A:** *Enpp2* expression in epididymal and BAT. *n* = 5 animals in each group. **B:** Serum ENPP2 levels. *n* = 8 animals in each group. **C:** Body weight changes in WT (gray lines) and Fat-*Enpp2* KO (black lines) mice fed an ND (broken lines) or high-fat diet (DIO, continuous lines). *n* = 8–10 animals in each group. §Fat-*Enpp2* KO ND vs. Fat-*Enpp2* KO DIO; †WT ND vs. WT DIO; *WT DIO vs. Fat-*Enpp2* DIO; *P* < 0.05. **D:** Daily food intake. *n* = 8 animals in each group. **E:** Weights of visceral epididymal, femoral subcutaneous, and interscapular brown fat pads. *n* = 8–10 animals in each group. **F:** Flow cytometric analysis of M1 macrophages (F4/80⁺CD11c⁺CD206⁺), M2 macrophages (F4/80⁺CD11c⁺CD206⁺), endothelial cells (EC), CD8⁺ T cells, CD4⁺ T cells, Pref1⁺CD34⁺ preadipocytes, Lin⁺CD29⁺CD90⁺ fibroblasts, and Lin⁺CD29⁺CD34⁺Sca1⁺ progenitors in SV fractions. *n* = 5 animals in each group. **G:** The BrdU⁺ cell fraction among Pref1⁺CD34⁺ preadipocytes in epididymal fat pads examined 3 days after BrdU injection. *n* = 5 animals in each group. **H:** AnnexinV⁺PI⁺ apoptotic cell fraction among Pref1⁺CD34⁺ preadipocytes in epididymal fat pads. *n* = 5 animals in each group. **P* < 0.05.

(Fig. 3J). This may reflect the stronger expression of *Ucp1*, *Ppargc1a*, *Cidea*, and *Mcpt1* in whole BAT from Fat-*Enpp2* KO mice than WT mice (Fig. 3K), as well as the increased BAT functionality and lipid oxidation capacity in Fat-*Enpp2* KO mice. The abovementioned difference in locomotion activity was not enough to fully explain the EE difference (20), and the unaltered food intake and thermogenic gene changes indicate that elevated energy dissipation reflecting more functional BAT also contributed to the improved metabolic phenotype.

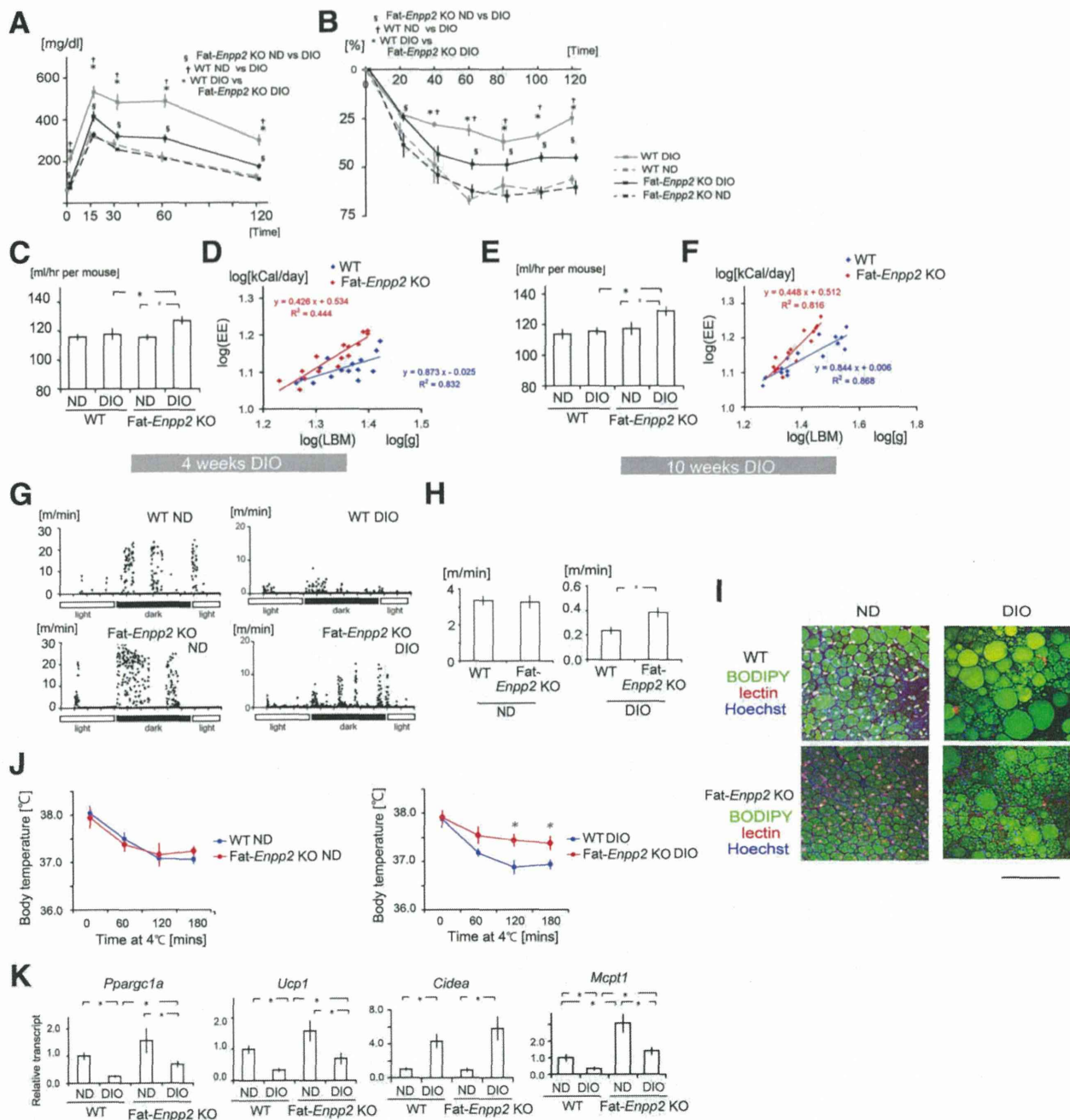


Figure 3—Adipocyte-specific *Enpp2* deletion improved BAT function, increased EE, and improved systemic metabolism. *Fat-Enpp2* KO and WT mice were fed either an ND or a high-fat diet (DIO) for 4 or 10 weeks. Mice were examined when they were 11 (4 weeks DIO) or 17 (10 weeks DIO) weeks old. Results of oral glucose tolerance (1 g/kg glucose) (A) and insulin tolerance (1 unit/kg insulin) (B) tests in 17-week-old WT (gray lines) and *Fat-Enpp2* KO (black lines) mice fed an ND (broken line) or high-fat diet (DIO, continuous line). *n* = 8–10 animals in each group. B: §*Fat-Enpp2* KO ND vs. *Fat-Enpp2* KO DIO; †WT ND vs. WT DIO; *WT DIO vs. *Fat-Enpp2* KO DIO; *P* < 0.05. O₂ consumption (*n* = 5 animals in each group) (after 4 weeks DIO [C] and after 10 weeks DIO [E]) and plot of EE and lean body mass index (LBM) (*n* = 20 animals in each group) (after 4 weeks DIO [D] and after 10 weeks DIO [F]). G and H: Representative and averaged locomotion in 17-week-old *Fat-Enpp2* KO and WT mice. *n* = 5 animals in each group. I: Histochemical identification of endothelial cells (lectin, red), adipocytes (BODIPY, green), and nuclei (Hoechst, blue) in brown adipose tissue from 17-week-old mice. J: Thermogenic responses in 17-week-old mice exposed to low temperature (4°C) conditions. Body core temperature was measured at the indicated times up to 3 h. *n* = 8 animals in each group. K: Real-time PCR analysis of mRNA expression of the indicated genes in whole (undigested) BAT from 17-week-old mice. The levels of each transcript were normalized to that in a lean control. *n* = 8 animals in each group. **P* < 0.05.

Adipocyte-Specific Overexpression of *Enpp2* Increases Adiposity

To further test whether ENPP2 expressed by adipocytes plays a role in metabolic control, we also generated a transgenic mouse line in which *Enpp2* was selectively overexpressed in adipocytes (Supplementary Fig. 6). Levels of ENPP2 expression were increased ~25-, 30-, and 15-fold in epididymal, inguinal, and BAT, respectively (Supplementary Fig. 6). Previous studies showed that the *Fabp4* (*aP2*) promoter may also drive transgene expression in macrophages and other cell types (21). When we analyzed *Enpp2* levels in macrophages within epididymal adipose tissue, we found that although *Enpp2* expression was increased, the level was <5% of that in adipocytes. Serum ENPP2 and LPA levels were increased fivefold in *Fabp4-Enpp2* transgenic mice (Supplementary Fig. 6). When fed a high-fat diet, the resultant *Fabp4-Enpp2* transgenic DIO mice showed greater body and fat pad weights than WT DIO mice and greater numbers of adipocytes in WAT (Supplementary Fig. 6).

Collectively, the effects of adipocyte-specific deletion and overexpression of *Enpp2* indicate that ENPP2 produced by adipocytes plays a key role in the development of adipose tissue obesity and the metabolic dysfunction induced by a high-fat diet.

ENPP2 Is Involved in Preadipocyte Hyperplasia and Differentiation

We then addressed the mechanism by which ENPP2 affects adipose tissue expansion. We hypothesized that ENPP2 positively affects adipocyte hyperplasia, and because adipocyte progenitor cell fractions were reduced in *Fat-Enpp2* KO DIO mice (Fig. 2F), we further hypothesized that ENPP2 is important for proliferation of adipocyte progenitors. Consistent with those ideas, recombinant ENPP2 promoted proliferation of 3T3-L1 cells, a line of Pref1⁺ CD34⁺ adipocyte progenitors (Fig. 4A–C). In addition, when subjected to hormonal stimulation, Pref1⁺ CD34⁺ adipocyte progenitors isolated from *Enpp2*^{+/-} WAT differentiated into lipid-bearing adipocytes less efficiently than WT preadipocytes (Fig. 4D–F).

We also examined the adipogenic gene expression profiles of isolated Pref1⁺ CD34⁺ preadipocytes in adipocyte-specific *Enpp2*-deficient mice and found that expression of *Cebpa*, *Cebpb*, *Cebpd*, and *Pparg* was reduced in preadipocytes from *Enpp2*-deficient mice (Fig. 4G). In addition, expression of *Klf5* and *Klf15*, two adipogenic transcriptional factors, was significantly reduced in these mice, whereas expression of the antiadipogenic factor *Klf2* was increased. Taken together, these results demonstrate that ENPP2 promotes preadipocyte proliferation and differentiation into adipocytes, thereby promoting adipocyte hyperplasia.

ENPP2 Promotes Preadipocyte Proliferation via Both LPA-Dependent and -Independent Mechanisms

ENPP2 may affect preadipocyte function through production of LPA and may also act directly, in an

LPA-independent manner, via its noncatalytic COOH-terminal domain (3). Consistent with an earlier report, we found that 5 μ mol/L LPA promoted proliferation and differentiation of Pref1⁺ CD34⁺ adipocyte progenitors from epididymal fat pads (22) (Fig. 4H–J). However, knockdown of LPA receptor 1 (EDG2), the main LPA receptor expressed by Pref1⁺ CD34⁺ adipocyte progenitors (Supplementary Fig. 7), only partially inhibited the effects of ENPP2 on the proliferation and differentiation of Pref1⁺ CD34⁺ adipocyte progenitors (Fig. 4A–C). By contrast, EDG2 knockdown almost completely blocked cell proliferation promoted by LPA (Fig. 4H–J). These results suggest that, in addition to LPA production, ENPP2 may affect preadipocyte function through LPA-EDG2-independent pathways.

To elucidate the contribution of *Enpp2* deficiency to functional LPA levels, we measured the interstitial concentration of LPA in epididymal fat using microdialysis catheters, as well as the serum levels (Supplementary Figs. 1 and 4). The interstitial levels measured in epididymal fat pad were lower in *Fat-Enpp2* KO mice than WT mice. We therefore speculated that ENPP2 contributes to local LPA levels within fat.

ENPP2 Released From Adipocytes Induces Macrophage and CD8⁺ T-Cell Activation

One of the striking phenotypes of global *Enpp2* haploinsufficiency and adipocyte-specific *Enpp2* deletion is the suppression of adipose tissue inflammation. Although this may be primarily due to the reduction in obesity, it is also possible that ENPP2 produced by adipocytes and progenitors modulates inflammatory processes independently of its effects on adipocyte hyperplasia. To begin to address the possible effects of adipocyte-derived ENPP2 on immune cells, we cocultured 3T3-L1 adipocytes and bone marrow-derived macrophages. The coculture increased expression of TNF- α in macrophages (Supplementary Fig. 8), but this effect was diminished by siRNA-mediated knockdown of *Enpp2* in the 3T3-L1 cells. In addition, recombinant ENPP2 increased TNF- α expression in macrophages. Recombinant ENPP2 also increased expression of CD44 and interferon- γ in CD8⁺ T cells in epididymal fat pads. These results indicate that ENPP2 from adipocytes contributes to immune cell function within epididymal fat pads, which is associated with adipose tissue inflammation in obesity.

Adipocyte *Enpp2* Expression Is Differentially Regulated During Adipocyte Differentiation and Hypertrophy

To gain further insight into the role of ENPP2 in the development of obesity, we analyzed the regulation of *Enpp2* expression in obese adipose tissue. Despite the fact that ENPP2 promotes obesity, the level of *Enpp2* expression was lower in both the SV and adipocyte fractions of WAT from 20-week-old DIO mice than from lean mice (Fig. 1B). This seeming discrepancy between the obesity-promoting function of ENPP2 and its downregulation in

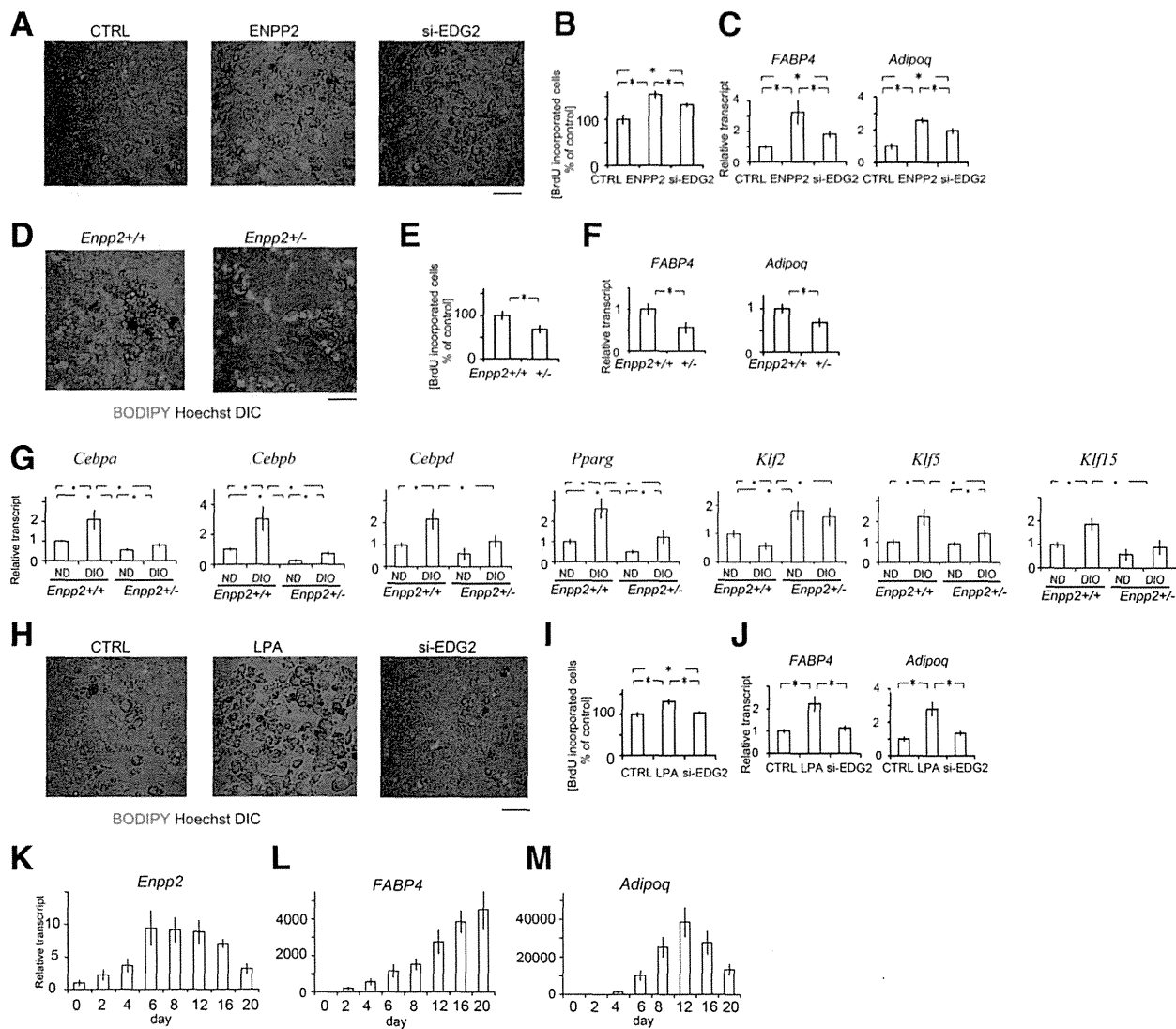


Figure 4—ENPP2 contributes to preadipocyte hyperplasia and adipocyte differentiation. Pref1⁺ CD34⁺ preadipocytes isolated from epididymal adipose tissue from 20-week-old WT mice (A–C) and *Enpp2*^{+/+} and *Enpp2*^{+/-} mice (D–F) were cultured and differentiated into adipocytes using hormonal stimulation. Accumulation of lipid droplets (A and D), cell proliferation (indicated by the number of BrdU⁺ cells) (B and E), and gene expression (C and F) are shown. *n* = 5 experiments in each group. A–C: Cells were treated with recombinant ENPP2 (10 ng/mL) and si-EDG2 and differentiated into adipocytes through hormonal stimulation for 48 h. D–F: Pref1⁺ CD34⁺ preadipocytes from *Enpp2*^{+/+} and *Enpp2*^{+/-} mice were also differentiated into adipocytes through hormonal stimulation for 96 h. G: Gene expression of Pref1⁺ CD34⁺ preadipocytes from epididymal fat pads of lean 20-week-old adipocyte-specific *Enpp2* KO and WT mice. *n* = 8–10 animals in each group. H–J: Pref1⁺ CD34⁺ preadipocytes isolated from WT mice were treated with LPA (1 μmol/L) and si-EDG2 and differentiated into adipocytes through hormonal stimulation for 48 h. Accumulation of lipid droplets (H), cell proliferation (I), and gene expression (J). K–M: *Enpp2*, *FABP4*, and *Adipoq* expression during differentiation of Pref1⁺ CD34⁺ preadipocytes. Expression from day 0 to 20 was examined. *n* = 5 experiments in each group. **P* < 0.05.

obese adipose tissue prompted us to further analyze *Enpp2* expression during adipocyte differentiation and hypertrophy. We first analyzed *Enpp2* expression in Pref1⁺ CD34⁺ adipocyte progenitor cells. Although *Enpp2* expression was increased during differentiation of Pref1⁺ CD34⁺ adipocyte progenitor cells, the levels peaked on day 6 and declined thereafter (Fig. 4K–M), suggesting *Enpp2* is upregulated in differentiating adipocytes but downregulated in hypertrophied adipocytes.

ENPP2 Expression in Subcutaneous Fat and Serum Levels Are Reduced in Obese Human Subjects

To further elucidate the role of ENPP2 in humans, we also measured ENPP2 expression in subcutaneous fat from human subjects. It was previously reported (23) that *EMR1* expression correlated positively with BMI (Supplementary Fig. 9), and we observed that ENPP2 expression was reduced in obese subjects (BMI >25.0). In addition, we used an ELISA-based, high-throughput system to assay

serum ENPP2 levels in large numbers of human samples (15). The results showed that serum ENPP2 levels are reduced in obese subjects, and multivariate analysis indicated ENPP2 to be an independent parameter associated with BMI (Supplementary Tables 1 and 2). Thus, the ENPP2 levels are also reduced in obese human subjects.

DISCUSSION

In the current study, we showed that ENPP2 contributes to the metabolic phenotype associated with obesity. We speculated that ENPP2 directly modulates the function of both BAT and WAT. EE and expression of *Ucp1* and *Ppargc1a* were higher in Fat-*Enpp2* KO mice than WT mice (Fig. 3). In addition, microscopic visualization showed that the numbers of multiple lipid droplet-containing adipocytes and mitochondrial membrane potential were increased in both mice. These results suggest that while BAT mass was smaller in Fat-*Enpp2* KO than WT DIO mice, the tissue remained functionally active. We therefore speculate that energy dissipation contributes to the improved metabolic profile and reduced weight gains seen in Fat-*Enpp2* KO mice fed a high-fat diet.

Enpp2 gene manipulation also affected the immune cell populations in adipose tissue and the tissue inflammation (Fig. 2F), and our finding that ENPP2 mediates proinflammatory interaction between 3T3-L1 adipocytes and macrophages suggests ENPP2 modulates immune cell function (Supplementary Fig. 8). Future studies will be needed to address the precise mechanisms by which ENPP2 contributes to the regulation of adipose tissue inflammation. Although we found no significant differences between the fibroblast fractions in *Enpp2*^{+/-} and *Enpp2*^{+/+} mice, or between their adipose *Colla1* or *Col6a1* expression, a contribution of fibrosis within fat pads to the phenotype of *Enpp2*-deficient mice could not fully be excluded (Supplementary Fig. 1).

It was revealed that ENPP2 has a functionally active COOH-terminal domain (i.e., the MORFO2 domain) that functions independently of ENPP2 catalytic activity and LPA production (3,24). In fact, LPA activity in preadipocyte proliferation and differentiation of Pref1⁺ CD34⁺ adipocyte progenitors was only partially inhibited by EDG2 knockdown (Fig. 4). However, the role of the MORFO2 domain in preadipocytes remains to be clarified.

Despite our finding that ENPP2 is important to adipose tissue obesity, its expression was diminished within obese adipose tissue and hypertrophied adipocytes (Fig. 1C and Fig. 4). On the other hand, it has also been reported that ENPP2 expression is elevated in adipose tissue from diabetic *db/db* mice and that DIO mice show no significant changes in ENPP2 expression (17). What's more, earlier studies produced contradictory results regarding BAT mass, locomotor activity, thermogenic profiles, and systemic metabolism (6,7). The precise mechanisms responsible for these discrepancies between the results of the current study and those earlier ones are not immediately clear, but there were several experimental

differences. First, all of our mouse models had a C57BL/6 genetic background. In study by Dusaulcy et al. (6), it appears the mice had a mixed genetic background (FVB and C57BL/6). This difference in genetic background could reportedly contribute to the difference in adipose phenotype between obese mice (25). In addition, we found that the distributions of immune cells in epididymal fat pads and BAT significantly differed between these two mouse strains (data not shown), and we speculate that the genetic differences also influenced the effects of *Enpp2* deficiency. Second, in Dusaulcy et al. (6), the mice were fed a high-fat diet for 13 weeks, starting when they were 10 weeks old. We started the high-fat diet when the mice were 7 weeks old because we found that early initiation of the diet was necessary to activate adipogenesis. In addition, levels of *Enpp2* expression in the SV and preadipocyte fractions peaked at 8 weeks of age and declined thereafter (data not shown). In our experiments, therefore, the mice were started on a high-fat diet while *Enpp2* levels were high, whereas in Dusaulcy's study, the high-fat diet was started after *Enpp2* levels had already declined to baseline. This difference in the timing of the high-fat diet may have led to the apparent difference in phenotypes. It is also possible that environmental factors affected the phenotypes. In fact, our examination showed that the effects of *Enpp2* deficiency on metabolic profiles depend on the timing of experiments during DIO (Supplementary Fig. 4H).

In humans, we found that serum ENPP2 levels correlated negatively with BMI and that levels of ENPP2 expression were reduced in subcutaneous fat from obese subjects (Supplementary Fig. 9). Earlier studies found that increases in adipocyte size correlated with serum insulin concentrations, insulin resistance, and increased risk of developing type 2 diabetes (26,27). Although in the current study we did not directly measure adipocyte size in human subjects, it is likely that levels of ENPP2 expression in obese subjects were negatively related to adipocyte size. Another possibility is that the progression of diabetes affects ENPP2 expression in adipose tissue. In fact, our preliminary analysis showed that there was a tendency toward higher serum ENPP2 levels in diabetic human subjects (data not shown).

In conclusion, our findings suggest that ENPP2 is a key mediator of adipose tissue obesity and is involved in the systemic regulation of BAT metabolism, and could be a useful therapeutic target for the treatment of metabolic disorders.

Acknowledgments. The authors thank Dr. Kotaro Yoshimura (Department of Plastic Surgery, Graduate School of Medicine, University of Tokyo) for human sample preparations and Dr. Hironori Waki (Department of Metabolic Diseases, University of Tokyo) for insightful comments on the manuscript. The authors also thank M. Tajima, C. Yoshinaga, X. Yingda, T. Hirabayashi (Department of Cardiovascular Medicine, University of Tokyo), C. Nakamikawa, and M. Ito (Center for Molecular Medicine, Jichi Medical University) for their excellent technical help.

Funding. This study was supported by research fellowships from the Japan Society for the Promotion of Science Research Fellowships for Young Scientists (S.N.); the Funding Program for World-Leading Innovative R&D on Science and Technology (FIRST Program) (S.N. and R.N.); Grants-in-Aid for Scientific Research (R.N.); grants from the Translational Systems Biology and Medicine Initiative (T.L. and R.N.) and the Global Centers of Excellence Program (T.K. and R.N.) from the Ministry of Education, Culture, Sports, Science and Technology of Japan; and a research grant from the National Institute of Biomedical Innovation (R.N.).

Duality of Interest. No potential conflicts of interest relevant to this article were reported.

Author Contributions. S.N. designed and performed experiments, analyzed data, and wrote the manuscript. M.N. performed experiments and reviewed the manuscript. S.O., T.O., R.O., K.N., and K.I. performed experiments. J.A. and Y.Y. performed experiments and contributed to discussion. H.Y., K.E., K.U., N.H., T.K., and I.K. contributed to discussion. R.N. directed this study. S.N. and R.N. are the guarantors of this work and, as such, had full access to all the data in the study and take responsibility for the integrity of the data and the accuracy of the data analysis.

References

1. Kadowaki T, Yamauchi T, Kubota N, Hara K, Ueki K, Tobe K. Adiponectin and adiponectin receptors in insulin resistance, diabetes, and the metabolic syndrome. *J Clin Invest* 2006;116:1784–1792
2. Hotamisligil GS. Inflammation and metabolic disorders. *Nature* 2006;444:860–867
3. Yuelling LM, Fuss B. Autotaxin (ATX): a multi-functional and multi-modular protein possessing enzymatic lysoPLD activity and matricellular properties. *Biochim Biophys Acta* 2008;1781:525–530
4. van Meeteren LA, Moolenaar WH. Regulation and biological activities of the autotaxin-LPA axis. *Prog Lipid Res* 2007;46:145–160
5. van Meeteren LA, Ruurs P, Stortelers C, et al. Autotaxin, a secreted lysophospholipase D, is essential for blood vessel formation during development. *Mol Cell Biol* 2006;26:5015–5022
6. Dusaulcy R, Rancoule C, Grès S, et al. Adipose-specific disruption of autotaxin enhances nutritional fattening and reduces plasma lysophosphatidic acid. *J Lipid Res* 2011;52:1247–1255
7. Federico L, Ren H, Mueller PA, et al. Autotaxin and its product lysophosphatidic acid suppress brown adipose differentiation and promote diet-induced obesity in mice. *Mol Endocrinol* 2012;26:786–797
8. Tanaka M, Okudaira S, Kishi Y, et al. Autotaxin stabilizes blood vessels and is required for embryonic vasculature by producing lysophosphatidic acid. *J Biol Chem* 2006;281:25822–25830
9. Liu D, Wen J, Liu J, Li L. The roles of free radicals in amyotrophic lateral sclerosis: reactive oxygen species and elevated oxidation of protein, DNA, and membrane phospholipids. *FASEB J* 1999;13:2318–2328
10. Nishimura S, Manabe I, Nagasaki M, et al. CD8⁺ effector T cells contribute to macrophage recruitment and adipose tissue inflammation in obesity. *Nat Med* 2009;15:914–920
11. Brake DK, Smith EO, Mersmann H, Smith CW, Robker RL. ICAM-1 expression in adipose tissue: effects of diet-induced obesity in mice. *Am J Physiol Cell Physiol* 2006;291:C1232–C1239
12. Nishimura S, Manabe I, Nagasaki M, et al. In vivo imaging in mice reveals local cell dynamics and inflammation in obese adipose tissue. *J Clin Invest* 2008;118:710–721
13. Camp HS, Chaudhry A, Leff T. A novel potent antagonist of peroxisome proliferator-activated receptor gamma blocks adipocyte differentiation but does not revert the phenotype of terminally differentiated adipocytes. *Endocrinology* 2001;142:3207–3213
14. Nishimura S, Manabe I, Nagasaki M, et al. Adipogenesis in obesity requires close interplay between differentiating adipocytes, stromal cells, and blood vessels. *Diabetes* 2007;56:1517–1526
15. Nakamura K, Igarashi K, Ide K, et al. Validation of an autotaxin enzyme immunoassay in human serum samples and its application to hypoalbuminemia differentiation. *Clin Chim Acta* 2008;388:51–58
16. van der Meer IM, Bots ML, Hofman A, del Sol AI, van der Kuip DA, Witteman JC. Predictive value of noninvasive measures of atherosclerosis for incident myocardial infarction: the Rotterdam Study. *Circulation* 2004;109:1089–1094
17. Boucher J, Quilliot D, Pradères JP, et al. Potential involvement of adipocyte insulin resistance in obesity-associated up-regulation of adipocyte lysophospholipase D/autotaxin expression. *Diabetologia* 2005;48:569–577
18. Lee KY, Russell SJ, Ussar S, et al. Lessons on conditional gene targeting in mouse adipose tissue. *Diabetes* 2013;62:864–874
19. Rodeheffer MS, Birsoy K, Friedman JM. Identification of white adipocyte progenitor cells in vivo. *Cell* 2008;135:240–249
20. Whittle AJ, Carobbio S, Martins L, et al. BMP8B increases brown adipose tissue thermogenesis through both central and peripheral actions. *Cell* 2012;149:871–885
21. Wang ZV, Deng Y, Wang QA, Sun K, Scherer PE. Identification and characterization of a promoter cassette conferring adipocyte-specific gene expression. *Endocrinology* 2010;151:2933–2939
22. Pagès G, Girard A, Jeanneton O, et al. LPA as a paracrine mediator of adipocyte growth and function. *Ann N Y Acad Sci* 2000;905:159–164
23. Weisberg SP, McCann D, Desai M, Rosenbaum M, Leibel RL, Ferrante AW Jr. Obesity is associated with macrophage accumulation in adipose tissue. *J Clin Invest* 2003;112:1796–1808
24. Dennis J, White MA, Forrest AD, et al. Phosphodiesterase-1alpha/autotaxin's MORFO domain regulates oligodendroglial process network formation and focal adhesion organization. *Mol Cell Neurosci* 2008;37:412–424
25. Haluzik M, Colombo C, Gavrilova O, et al. Genetic background (C57BL/6J versus FVB/N) strongly influences the severity of diabetes and insulin resistance in ob/ob mice. *Endocrinology* 2004;145:3258–3264
26. Lundgren M, Svensson M, Lindmark S, Renström F, Ruge T, Eriksson JW. Fat cell enlargement is an independent marker of insulin resistance and 'hyperleptinaemia'. *Diabetologia* 2007;50:625–633
27. Arner E, Westermark PO, Spalding KL, et al. Adipocyte turnover: relevance to human adipose tissue morphology. *Diabetes* 2010;59:105–109

ARTICLE

Received 3 Jun 2014 | Accepted 13 Aug 2014 | Published 19 Sep 2014

DOI: 10.1038/ncomms5982

Macrophage-inducible C-type lectin underlies obesity-induced adipose tissue fibrosis

Miyako Tanaka^{1,*}, Kenji Ikeda^{1,*}, Takayoshi Suganami^{2,3}, Chikara Komiya¹, Kozue Ochi¹, Ibuki Shirakawa², Miho Hamaguchi¹, Satoshi Nishimura^{4,5,6}, Ichiro Manabe⁴, Takahisa Matsuda⁷, Kumi Kimura⁸, Hiroshi Inoue⁸, Yutaka Inagaki⁹, Seiichiro Aoe¹⁰, Sho Yamasaki¹¹ & Yoshihiro Ogawa¹

In obesity, a paracrine loop between adipocytes and macrophages augments chronic inflammation of adipose tissue, thereby inducing systemic insulin resistance and ectopic lipid accumulation. Obese adipose tissue contains a unique histological structure termed crown-like structure (CLS), where adipocyte-macrophage crosstalk is known to occur in close proximity. Here we show that Macrophage-inducible C-type lectin (Mincle), a pathogen sensor for *Mycobacterium tuberculosis*, is localized to macrophages in CLS, the number of which correlates with the extent of interstitial fibrosis. Mincle induces obesity-induced adipose tissue fibrosis, thereby leading to steatosis and insulin resistance in liver. We further show that Mincle in macrophages is crucial for CLS formation, expression of fibrosis-related genes and myofibroblast activation. This study indicates that Mincle, when activated by an endogenous ligand released from dying adipocytes, is involved in adipose tissue remodelling, thereby suggesting that sustained interactions between adipocytes and macrophages within CLS could be a therapeutic target for obesity-induced ectopic lipid accumulation.

¹Department of Molecular Endocrinology and Metabolism, Graduate School of Medical and Dental Sciences, Tokyo Medical and Dental University, Tokyo 113-8510, Japan. ²Department of Organ Network and Metabolism, Graduate School of Medical and Dental Sciences, Tokyo Medical and Dental University, Tokyo 113-8510, Japan. ³Japan Science and Technology Agency, PRESTO, Tokyo, Japan. ⁴Department of Cardiovascular Medicine, The University of Tokyo, Tokyo 113-8655, Japan. ⁵Translational Systems Biology and Medicine Initiative, The University of Tokyo, Tokyo 113-8655, Japan. ⁶Jichi Medical University, Tochigi 329-0498, Japan. ⁷Pharmaceutical Research Division, Takeda Pharmaceutical Company, Fujisawa 251-8555, Japan. ⁸Department of Physiology and Metabolism, Brain/Liver Interface Medicine Research Center, Kanazawa University, Kanazawa 920-8641, Japan. ⁹Department of Regenerative Medicine, Center for Matrix Biology and Medicine, Tokai University School of Medicine, Isehara 259-1193, Japan. ¹⁰Department of Home Economics, Otsuma Women's University, Tokyo 102-8357, Japan. ¹¹Division of Molecular Immunology, Medical Institute of Bioregulation, Kyushu University, Fukuoka 812-8582, Japan. * These authors contributed equally to this work. Correspondence and requests for materials should be addressed to T.S. (email: suganami.mem@tmd.ac.jp) or to Y.O. (email: ogawa.mem@tmd.ac.jp).

Obesity is a state of chronic, low-grade inflammation^{1,2}. Indeed, adipose tissue in obesity is characterized by adipocyte hypertrophy, followed by increased angiogenesis, immune cell infiltration, extracellular matrix overproduction, which is referred to as 'adipose tissue remodelling'^{3,4}. As a molecular mechanism, we have provided evidence that a paracrine loop involving saturated fatty acids and tumour necrosis factor- α (TNF α) derived from adipocytes and macrophages, respectively, establishes a vicious cycle, thereby accelerating the inflammatory change in obese adipose tissue⁵. It is conceivable that increased adipose tissue inflammation stimulates adipocyte lipolysis and tissue fibrosis, and thus enhances the release of free fatty acids from the adipose tissue, which may be accumulated in non-adipose tissue such as liver and skeletal muscle, as ectopic fat, and induce a variety of metabolic abnormalities called lipotoxicity^{3,4}. In this regard, Khan *et al.*⁶ reported that mice lacking collagen VI, which is expressed abundantly in adipose tissue, exhibit the uninhibited adipose tissue expansion and substantial improvement in insulin sensitivity on a high-fat diet (HFD). Although recent evidence suggests a role for obesity-induced hypoxic state^{7,8}, the molecular mechanisms underlying adipose tissue fibrosis are still largely unknown.

As the site of crosstalk between adipocytes and macrophages, there is a unique structure in obese adipose tissue called crown-like structure (CLS), where macrophages are considered to scavenge the residual lipid droplets of dead adipocytes^{9,10}. Histologically, proinflammatory M1 macrophages aggregate to constitute CLS in obese adipose tissue of humans and rodents. On the other hand, M2 macrophages are scattered in the interstitial spaces between adipocytes¹⁰. Notably, the number of CLS is positively correlated with systemic insulin resistance in obese subjects^{11,12}, suggesting the pathophysiologic role of CLS in adipose tissue inflammation and systemic energy metabolism. However, how CLS is formed in adipose tissue during the course of obesity and how it is involved in adipose tissue remodelling are poorly understood.

Macrophage-inducible C-type lectin (Mincle, Clec4e or Clec5f9) is a pathogen sensor that recognizes pathogenic fungi and *Mycobacterium tuberculosis*^{13–16}, and as the name implies, it is induced in macrophages by lipopolysaccharide through Toll-like receptor 4 (TLR4; ref. 17). We previously reported that saturated fatty acids also induce *Mincle* expression in macrophages through TLR4 (ref. 18). Moreover, the obesity-induced increase in *Mincle* expression in adipose tissue is markedly attenuated in C3H/HeJ mice with defective TLR4 signalling relative to control C3H/HeN mice¹⁸. Yamasaki *et al.* reported that Mincle can sense cell death as well to induce proinflammatory cytokine production and suggested the role of Mincle in sterile inflammation¹⁹. We have recently demonstrated that *Mincle* is induced in adipose tissue macrophages during the interaction between adipocytes and macrophages, at least partly, through the saturated fatty acid/TLR4/NF- κ B pathway¹⁸. It is currently unclear whether Mincle regulates adipose tissue inflammation and thus systemic energy metabolism in obesity, and if so, how it does remains to be elucidated.

Here we show that *Mincle*, when induced during the development of obesity, is localized to macrophages constituting CLS in adipose tissue. Interestingly, *Mincle* KO mice are protected against obesity-induced CLS formation and adipose tissue fibrosis, followed by reduced ectopic lipid accumulation and insulin resistance in the liver. On the other hand, treatment with trehalose-6,6'-dimycolate (TDM), a mycobacterial cell wall glycolipid that is known to be a Mincle ligand¹³, induces CLS formation and interstitial fibrosis in adipose tissue in mice. Mincle stimulation also induces potentially expression of

fibrosis-related genes in macrophages *in vitro*. This study provides evidence that Mincle has a role in the crosstalk between adipocytes and macrophages in CLS, thereby leading to activation of fibrogenic programme. Our data also suggest that antagonism of Mincle in macrophages offers a novel therapeutic strategy to prevent or treat obesity-induced adipose tissue fibrosis and thus ectopic lipid accumulation.

Results

Adipose tissue *Mincle* expression in obesity. We previously reported that *Mincle* expression is markedly upregulated in adipose tissue macrophages in obesity¹⁸. In this study, we first examined the time course of *Mincle* mRNA expression in epididymal fat tissue of wild-type mice fed a HFD and found that *Mincle* mRNA expression was roughly constant in wild-type mice fed a standard diet (SD) throughout the experimental period. On the other hand, *Mincle* mRNA expression was significantly increased in wild-type mice fed a HFD relative to those fed a SD at 16 weeks and gradually increased up to 50 weeks. There was no significant difference in expression of *Emr1*, which encodes macrophage marker F4/80, between 16 and 50 weeks (Fig. 1a). *Mincle* mRNA expression was also increased in liver to a lesser extent than epididymal fat tissue (Fig. 1b). At 16 weeks, *Mincle* mRNA expression was markedly high in epididymal fat tissue relative to subcutaneous fat tissue, which was roughly in parallel with *Emr1* mRNA expression (Fig. 1c). In the stromal-vascular fraction (SVF) from epididymal fat tissue of genetically obese *ob/ob* mice, *Mincle* mRNA was exclusively expressed in CD45⁺CD11b⁺F4/80⁺ cells or macrophages (Fig. 1d). In line with this, flow cytometric analysis revealed that obesity markedly increased the number of Mincle-positive macrophages, whereas there was no appreciable *Mincle* expression in other immune cells (Fig. 1e).

Altered lipid distribution in *Mincle* KO mice. We next examined the metabolic phenotypes of *Mincle* KO mice at 16 weeks of HFD feeding. There was no appreciable difference in body weight and subcutaneous fat weight between the genotypes (Fig. 2a and Supplementary Fig. 1a). The epididymal fat weight was significantly increased with reciprocal reduction of the liver weight in *Mincle* KO mice relative to wild-type mice on a HFD (Fig. 2a and Supplementary Fig. 1a). Histological examination revealed that hepatic steatosis was markedly attenuated in *Mincle* KO mice relative to wild-type mice (Fig. 2b). Consistently, hepatic triglyceride content and serum free fatty acid (FFA) and alanine aminotransferase (ALT) concentrations were significantly reduced in *Mincle* KO mice relative to wild-type mice (Fig. 2c,d). Basically, similar results were obtained in *Mincle* KO mice fed a HFD for 50 weeks (Supplementary Fig. 2a,b). On the other hand, at 8 weeks of HFD feeding when there was no apparent difference in *Mincle* expression in epididymal fat tissue between the diets (Fig. 1a), we did not observe any difference in the body weight and tissue weights between the genotypes (Supplementary Fig. 3). These observations suggest the altered lipid distribution in adipose tissue and liver in *Mincle* KO mice on a HFD.

Ameliorated glucose metabolism in *Mincle* KO mice. We performed the glucose tolerance test at 16 weeks of HFD feeding and found that *Mincle* KO mice showed better glucose tolerance and lower serum insulin concentrations than wild-type mice (Supplementary Fig. 1b). Moreover, the insulin-induced phosphorylation of Akt was significantly increased in the liver of *Mincle* KO mice relative to that of wild-type mice (Supplementary Fig. 1c). The phosphorylated Akt levels also tended to increase in the adipose tissue and skeletal muscle in *Mincle* KO mice, which

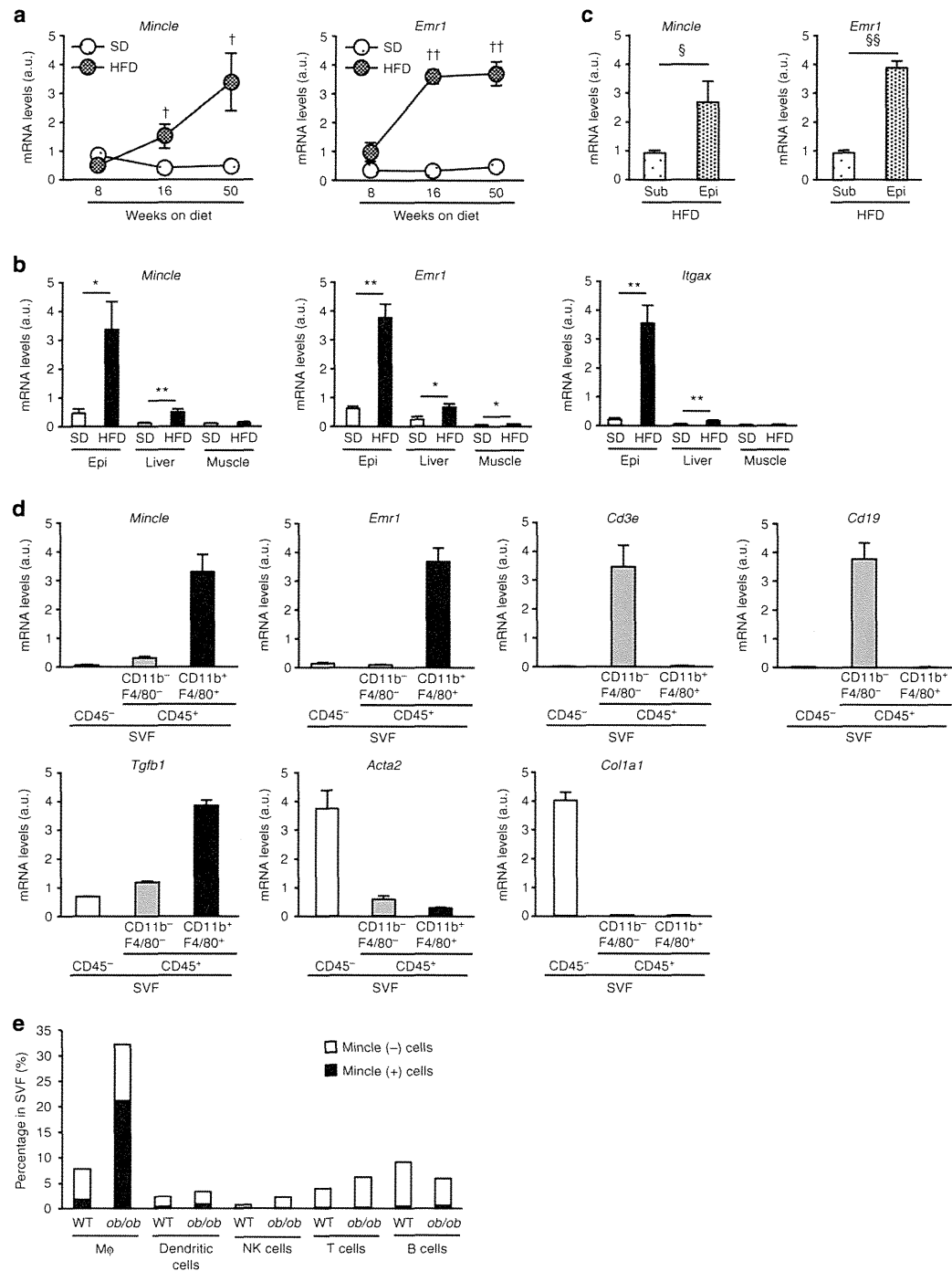


Figure 1 | Adipose tissue *Mincle* expression and *Mincle*-expressing cells in obese adipose tissue. (a) Time course of *Mincle* mRNA and *Emr1* (F4/80) expression in epididymal fat tissue of wild-type mice fed a HFD or a SD for up to 50 weeks. Values are mean \pm s.e.m. The data are analysed by unpaired *t*-test; $n = 5$ to 11 ; $^{\dagger}P < 0.05$, $^{\dagger\dagger}P < 0.01$ versus SD at each time point. (b) mRNA expression of *Mincle*, *Emr1* and *Itgax* (CD11c) in epididymal fat tissue (Epi), liver and skeletal muscle in wild-type mice fed a HFD for 50 weeks. Values are mean \pm s.e.m. The data are analysed by unpaired *t*-test; $n = 5$ to 10 ; $^*P < 0.05$, $^{**}P < 0.01$. (c) *Mincle* mRNA expression in epididymal (Epi) and subcutaneous (Sub) fat tissues of wild-type mice on a HFD for 16 weeks. Values are mean \pm s.e.m. The data are analysed by unpaired *t*-test; $n = 11$; $^{\S}P < 0.05$, $^{\S\S}P < 0.01$. (d) mRNA expression of *Mincle*, *Emr1*, *Acta2* (α SMA), and other cell type markers in CD45⁻, CD45⁺CD11b⁻ F4/80⁻ and CD45⁺CD11b⁺ F4/80⁺ cells isolated from SVF. Values are mean \pm s.e.m.; $n = 4$. (e) Percentage of *Mincle*-expressing cells in various immune cells in SVF. Values are the average of four samples.

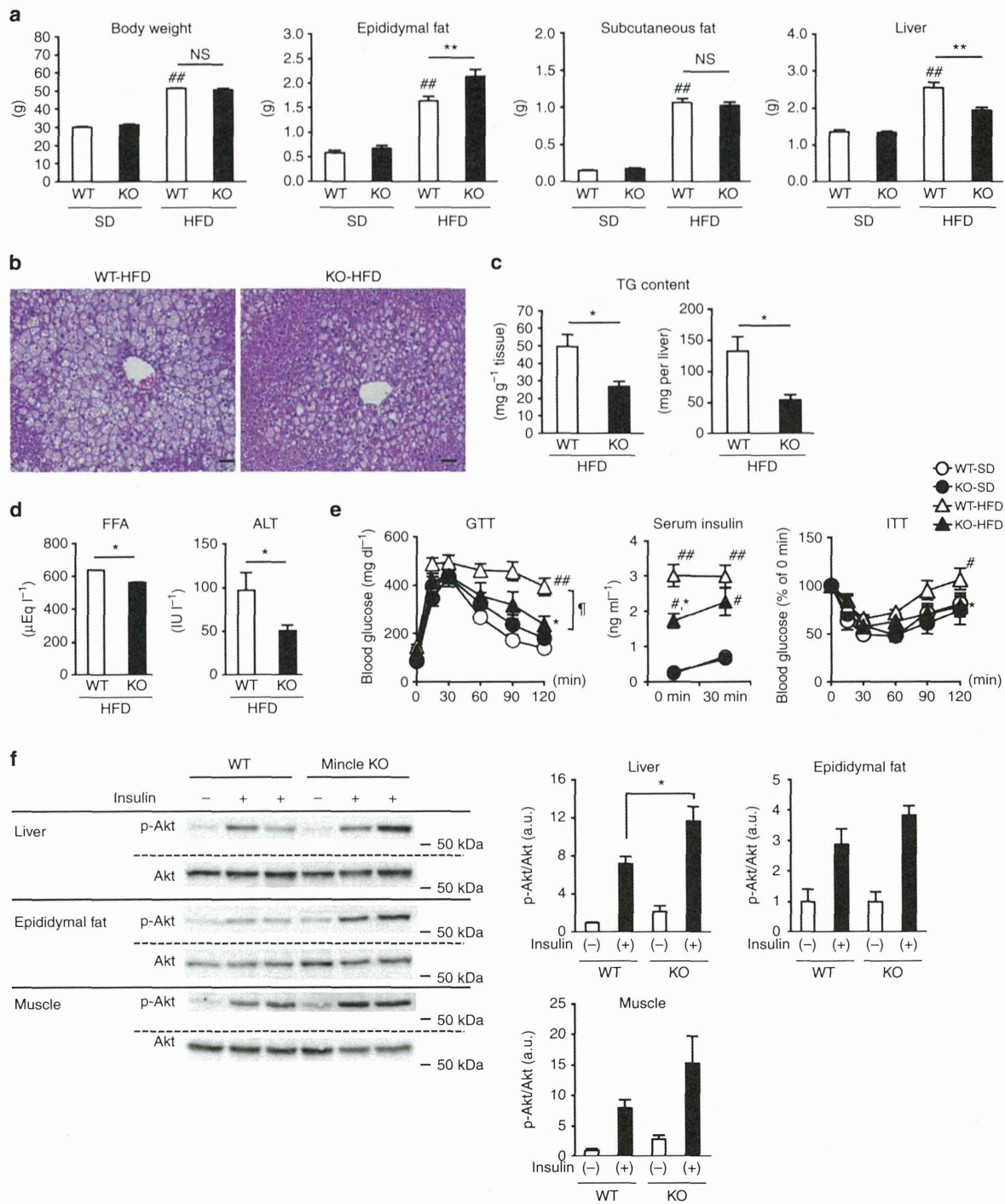


Figure 2 | Altered lipid distribution between adipose tissue and liver in Mincle KO mice. (a) Body weight and fat and liver weights of Mincle KO and wild-type mice at 16 weeks. Values are mean \pm s.e.m. The data are analysed by analysis of variance (ANOVA) followed by Tukey-Kramer test. ## P < 0.01 versus WT-SD, ** P < 0.01. NS, not significant; n = 11 to 13. (b–d) Representative hematoxylin and eosin staining of the liver (b), hepatic triglyceride (TG) content (c) and serum FFA and ALT concentrations (d) in Mincle KO and wild-type mice at 16 weeks. Original magnification, \times 200; Scale bar, 50 μ m. Values are mean \pm s.e.m. The data are analysed by unpaired t -test. * P < 0.05; n = 11 to 13. (e,f) Glucose metabolism in Mincle KO and wild-type mice fed a HFD for 50 weeks; n = 5 to 8. (e) Glucose and insulin tolerance tests. Values are mean \pm s.e.m. The data are analysed by ANOVA followed by Tukey-Kramer test. # P < 0.05, ## P < 0.01 versus WT-SD and * P < 0.05 versus WT-HFD at each point. † P < 0.05 assessed by ANOVA with repeated-measures analysis. (f) Western blotting of phosphorylated Akt (Thr308) in liver, epididymal fat tissue and soleus muscle. Values are mean \pm s.e.m. The data are analyzed by ANOVA followed by Tukey-Kramer test; * P < 0.05.

did not reach statistical significance. In addition, there was a slight decrease in the insulin-positive area and the number of Ki67-positive cells in the pancreas of *Mincle* KO mice relative to that of wild-type mice, whereas the islet area and glucagon-positive area did not differ between the genotypes (Supplementary Fig. 4). These observations suggest that reduced insulin resistance in the liver leads to better glucose tolerance in *Mincle* KO mice. We confirmed similar results at 50 weeks (Fig. 2e,f and Supplementary Fig. 2c). Collectively, HFD-induced insulin resistance was ameliorated in the liver of *Mincle* KO mice along with reduced hepatic lipid accumulation.

Reduced adipose tissue fibrosis in *Mincle* KO mice. Histological analysis of epididymal fat tissue revealed that adipocyte cell size appears to be increased in *Mincle* KO mice relative to wild-type mice on a HFD for 16 weeks, whereas there was no significant difference in the number of adipocytes (Fig. 3a). In this study, mRNA expression of genes related to adipogenesis, lipogenesis, lipolysis and β -oxidation did not differ between the genotypes (Supplementary Fig. 5). In addition, flow cytometric analysis showed no significant difference in the ratio of each immune cell to the SVF (Supplementary Fig. 6). On the other hand, Masson's trichrome staining revealed extensive interstitial fibrosis in epididymal fat tissue of wild-type mice, which is markedly suppressed in *Mincle* KO mice (Fig. 3b,c). We also obtained similar results by Sirius red staining and measurement of total collagen content (Fig. 3d–f). Consistently, there was a significant decrease in the area of α SMA-positive cells or myofibroblasts in *Mincle* KO mice relative to wild-type mice (Fig. 3g,h). Interestingly, there was no significant difference in total collagen content of subcutaneous fat tissue between the genotypes (Fig. 3f). We confirmed these results in *Mincle* KO mice fed a HFD for 50 weeks (Supplementary Fig. 2d,e). Collectively, these observations indicate reduced interstitial fibrosis in epididymal fat tissue of *Mincle* KO mice relative to wild-type mice.

Since *Mincle* is expressed selectively in adipose tissue macrophages (Fig. 1e), we next performed bone marrow transplantation (BMT) experiments to confirm the role of *Mincle* in bone marrow-derived cells. In this study, the substitution rate of BMT was more than 90% (Supplementary Fig. 7a). *Mincle* mRNA expression in epididymal fat tissue was almost negligible in bone marrow-specific *Mincle* KO mice (*Mincle* KO-BM mice) compared with the control mice (EGFP-BM mice) (Supplementary Fig. 7b), suggesting the macrophage-selective expression of *Mincle* (Fig. 1d). Under these experimental conditions, we confirmed that *Mincle* deficiency protected against HFD-induced adipose tissue fibrosis (Supplementary Fig. 7c).

Reduced CLS formation in adipose tissue of *Mincle* KO mice.

To determine the localization of *Mincle* expression in obese adipose tissue, we performed *in situ* hybridization analysis and found that *Mincle* occurs in some of the macrophages constituting CLS in epididymal fat tissue (Fig. 4a,b). Flow cytometric analysis revealed that CD11b⁺F4/80^{lo} cells isolated from the SVF showed higher *Mincle* mRNA expression than CD11b⁺F4/80^{hi} cells (Fig. 4c). CD11b⁺F4/80^{lo} cells expressed higher *Itgax* (CD11c) and lower *Mrc1* (CD206) mRNA levels than CD11b⁺F4/80^{hi} cells. These observations are consistent with our previous data that *Mincle* is expressed selectively in proinflammatory M1 macrophages *in vitro*¹⁸. Interestingly, the CLS density in *Mincle* KO mice was markedly reduced relative to wild-type mice (Fig. 4d,e). Moreover, there was a significant decrease in *Tnfa* (TNF α) mRNA expression in *Mincle* KO mice relative to wild-type mice on a HFD (Fig. 4f). On the other hand, there was

no significant difference in macrophage number (Fig. 4e) and polarization (Fig. 4f and Supplementary Fig. 6b) between the genotypes. By double-immunofluorescent staining of F4/80 (green) and collagen I (red), we observed the adjacent spatial relationship between CLS and fibrotic regions (Fig. 4g). The CLS density was positively correlated with the extent of adipose tissue fibrosis determined by Masson's trichrome and Sirius red stainings (Fig. 4h). Collectively, these observations suggest that *Mincle*-mediated CLS formation has a role in interstitial fibrosis in adipose tissue.

Mincle-stimulated fibrogenic gene expression in macrophages.

To elucidate how *Mincle* regulates adipose tissue fibrosis, we performed DNA microarray analysis of peritoneal macrophages stimulated with TDM (Fig. 5a). A total of 179 genes were up-regulated by TDM in wild-type macrophages and the effect was totally abolished in *Mincle* KO macrophages (Supplementary Table 1), indicating the *Mincle*-specific activation by TDM. In addition to known chemokine and cytokine genes, pathway analysis using Reactome database (<http://www.reactome.org/>) identified several large clusters related to tissue remodelling (Supplementary Fig. 8). By quantitative real-time PCR, we confirmed that TDM treatment markedly increases mRNA expression of *Tgfb1* (TGF β 1), *Pdgfb* and *Timp1* (Fig. 5b), which regulate extracellular matrix (ECM) production, fibroblast proliferation and ECM degradation, respectively²⁰. Since the Fc receptor common γ -chain (FcR γ)-spleen tyrosine kinase (Syk) cascade is shown to be downstream of *Mincle* signalling¹⁹, we examined the involvement of Syk in the induction of fibrosis-related genes. Treatment with a Syk-inhibitor suppressed dose-dependently the mRNA expression of *Tgfb1*, *Pdgfb* and *Timp1* along with *Cxcl2* (MIP-2), a chemokine that is induced by the *Mincle*-Syk pathway¹⁹ (Fig. 5c). These observations suggest that *Mincle* activation potentially induces fibrosis-related genes through Syk in macrophages.

Mincle-stimulated increase of myofibroblasts in SVF.

Since activated fibroblasts or myofibroblasts are crucial for fibrogenesis in various tissues and organs^{20,21}, we next examined the effect of *Mincle* stimulation of SVF that contains a variety of cell types such as immune cells, vascular cells and fibroblasts (Fig. 6a). The SVF was prepared from epididymal fat tissue of 9-week-old *ob/ob* mice; they showed high macrophage infiltration and *Mincle* expression relative to wild-type mice as reported¹⁸. Stimulation with TDM for 1 day significantly increased *Mincle*, *Tnfa*, *Pdgfb* and *Timp1* mRNA expression in the SVF (Fig. 6b). The effect of *Mincle* stimulation was also observed after 3 days (Fig. 6b). Interestingly, mRNA expression of *Acta2*, which encodes the myofibroblast marker α SMA, was significantly increased by *Mincle* stimulation (Fig. 6b). To address the effect of *Mincle* activation in macrophages on adipose tissue fibroblasts, we co-cultured peritoneal macrophages with CD45⁺CD31[−] cells prepared from the SVF of *ob/ob* mice which should abundantly include fibroblasts (Fig. 6c). Stimulation of the co-culture with TDM time-dependently increased mRNA expression of *Acta2*, which was followed by the increase of *Col1a1* (collagen I) mRNA expression (Fig. 6d). These observations strongly suggest that *Mincle* activation in macrophages effectively increases the number of myofibroblasts in adipose tissue.

***Mincle*-stimulated interstitial fibrosis in adipose tissue.** We next examined whether stimulation of *Mincle* is sufficient to induce interstitial fibrosis in adipose tissue *in vivo*. Emulsion containing TDM or vehicle was injected directly into epididymal

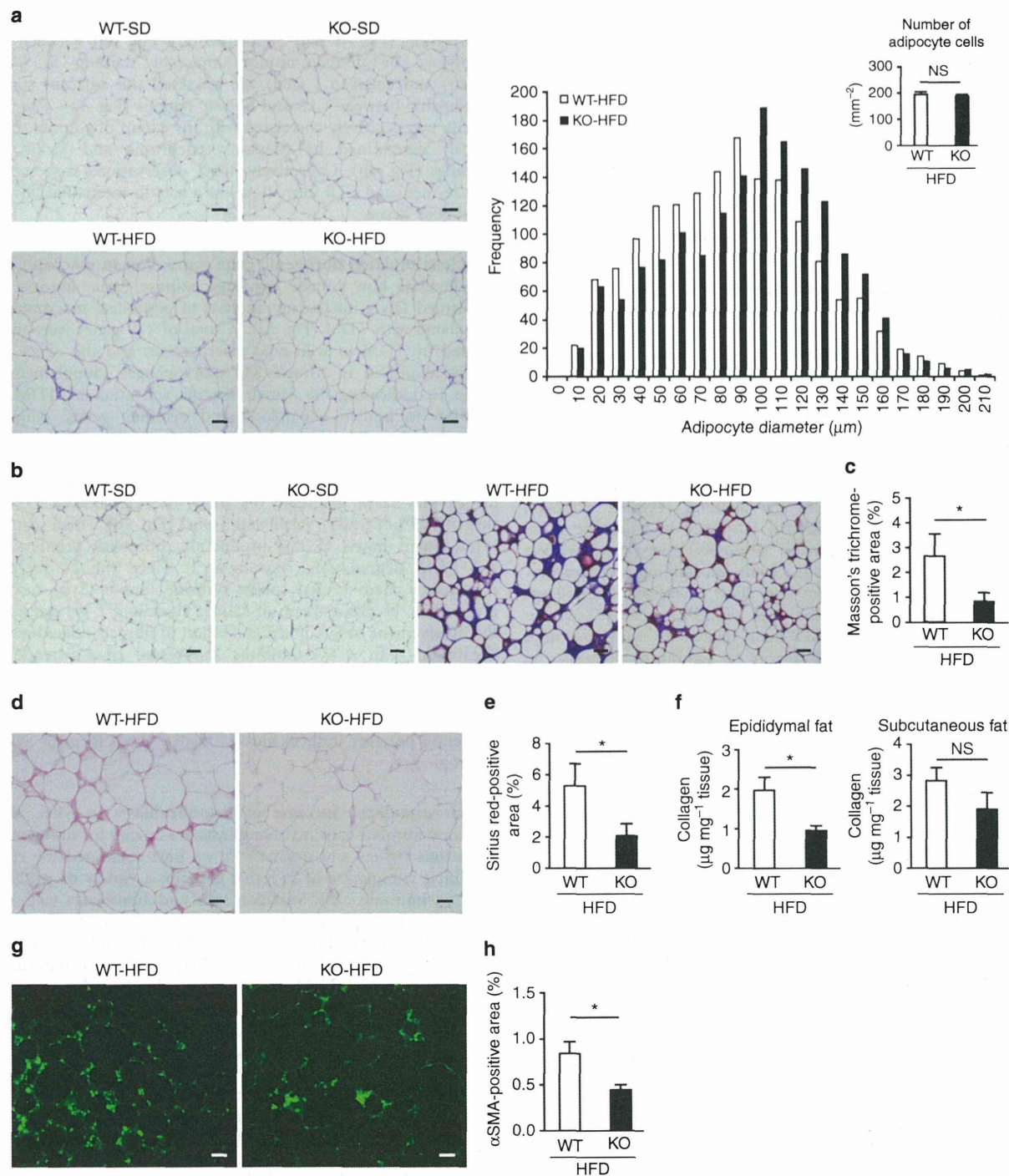


Figure 3 | Reduced interstitial fibrosis in adipose tissue of *Mincle* KO mice. *Mincle* KO and wild-type mice were fed a HFD or a SD for 16 weeks. (a) Representative hematoxylin and eosin staining, the histogram of adipocyte diameters in epididymal fat tissue. Inset, the number of adipocyte cells in epididymal fat tissue. (b,c) Representative Masson's trichrome staining (b) and quantification of Masson's trichrome-positive area (identical with interstitial fibrosis) (c) in epididymal fat tissue. (d,e) Representative Sirius red staining (d) and quantification of Sirius red-positive area (e) in epididymal fat tissue. (f) Total collagen contents in epididymal and subcutaneous fat tissues. (g,h) Representative α SMA staining (g) and quantification of α SMA-positive area (h) in epididymal fat tissue. Original magnification, $\times 200$; Scale bar, 50 μ m. Values are mean \pm s.e.m. The data are analysed by unpaired *t*-test. **P* < 0.05; NS, not significant; *n* = 11 to 13.

fat tissue of *Mincle* KO and wild-type mice on a SD. Seven days after the injection, Masson's trichrome staining revealed extensive interstitial fibrosis in TDM-treated wild-type mice, which was markedly suppressed in TDM-treated *Mincle* KO mice (Fig. 7a,b). By immunofluorescent staining, TDM-treated wild-type mice exhibited the CLS formation, where macrophage-surrounding

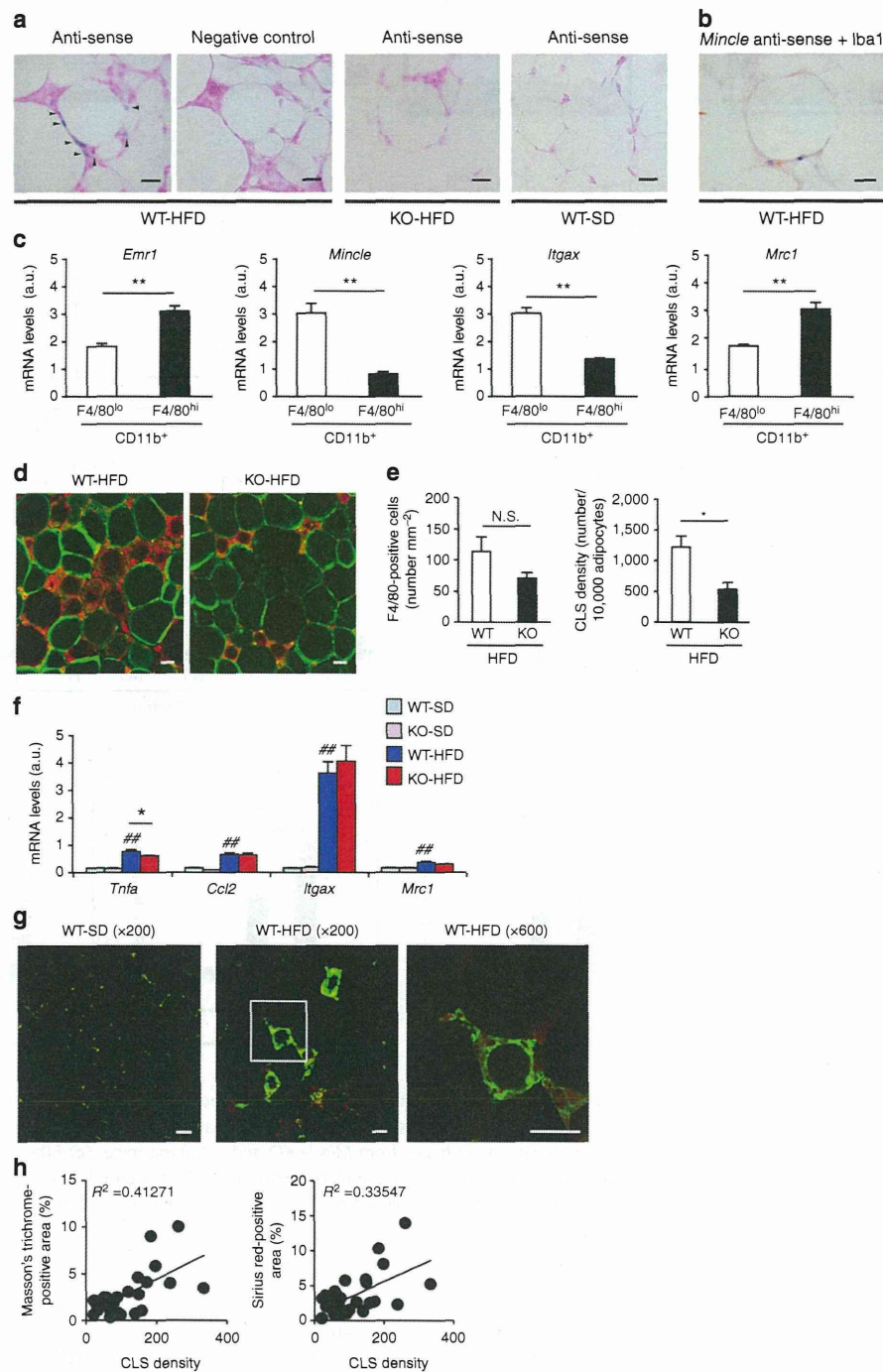
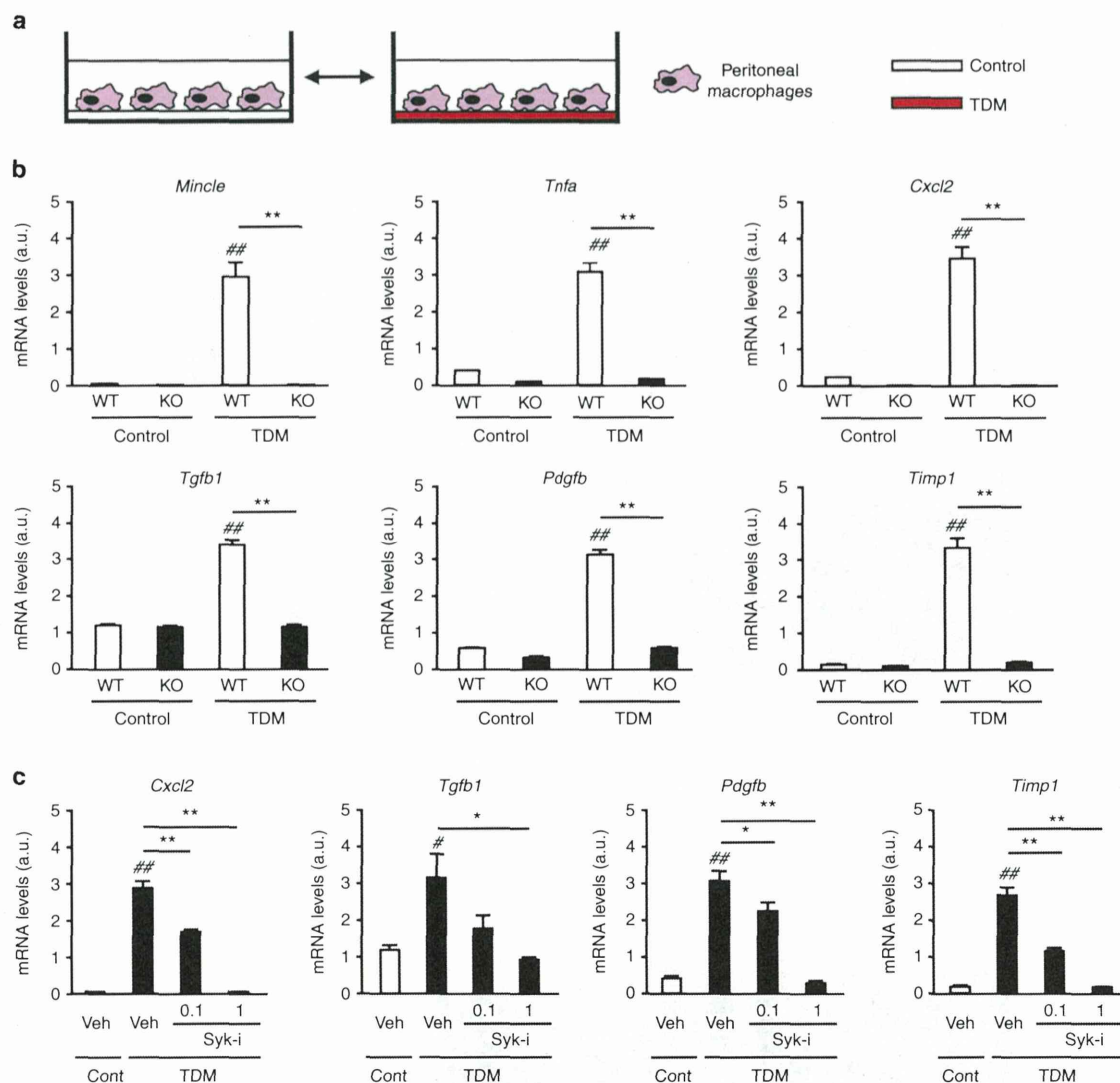


Figure 4 | Reduced CLS formation in adipose tissue of *Mincle* KO mice. (a) Representative *in situ* hybridization for *Mincle* mRNA in epididymal fat tissue of wild-type and *Mincle* KO mice fed a HFD for 16 weeks. The sections were hybridized with an anti-sense or a sense probe. (b) Double staining for *Mincle* (blue) and Iba1, a macrophage marker (brown). After *in situ* hybridization for *Mincle* mRNA, the sections were immunostained with an anti-Iba1 antibody. Original magnification, $\times 400$; Scale bars, 25 μm . (c) mRNA expression of *Mincle*, *Emr1*, *Itgax* and *Mrc1* (CD206) in CD11b⁺ F4/80^{lo} and CD11b⁺ F4/80^{hi} cells isolated from SVF. Values are mean \pm s.e.m. The data are analysed by unpaired *t*-test; $n = 4$, $**P < 0.01$. (d,e) Representative immunofluorescent staining of F4/80 (red) and perilipin (green) (d) and the number of F4/80-positive cells and crown-like structure (CLS) density (e) in epididymal fat tissue of *Mincle* KO and wild-type mice fed a HFD for 16 weeks. Original magnification, $\times 200$; Scale bars, 50 μm . Values are mean \pm s.e.m. The data are analysed by unpaired *t*-test; $n = 6$ to 8, $*P < 0.05$. NS, not significant. (f) mRNA expression of *Tnfa* (TNF α), *Ccl2* (MCP-1), *Itgax* and *Mrc1* in epididymal fat tissue of *Mincle* KO and wild-type mice fed a HFD for 16 weeks. Values are mean \pm s.e.m. The data are analysed by ANOVA followed by Tukey-Kramer test. $n = 5$ to 11. $##P < 0.01$ versus WT-SD, $*P < 0.05$. (g) Representative immunofluorescent staining of F4/80 (green) and collagen I (red) in epididymal fat tissue of wild-type mice fed a SD or a HFD for 16 weeks. Scale bar, 50 μm . (h) Linear regression analysis of correlations between Masson's trichrome- or Sirius red-positive area and CLS density in epididymal fat tissue of wild-type mice fed a HFD for 16 to 20 weeks; $n = 24$.



adipocytes were negative for perilipin staining, which was closely associated with collagen deposition (Fig. 7c). Moreover, we injected the emulsion into epididymal fat tissue of COL/EGFP transgenic (Tg) mice, which express EGFP exclusively in collagen I-producing cells. We observed that a number of EGFP-positive cells were accumulated around the CLS in TDM-treated mice (Fig. 7d). In TDM-treated wild-type mice, *Mincle* and *Itgax* mRNA expression was markedly induced throughout the experimental period, whereas *Mrc1* mRNA expression was gradually decreased (Fig. 7e). mRNA expression of *Acta2* and collagen was gradually increased up to day 7 (Fig. 7f). Notably, there was no upregulation of these genes in TDM-treated *Mincle* KO mice (Fig. 7f). Collectively, these observations suggest that *Mincle* stimulation is capable of inducing interstitial fibrosis in adipose tissue *in vivo*.

Discussion

Since numerous studies have shown that obesity induces chronic inflammation in adipose tissue^{1,2}, it is not surprising that, similar to various organs and tissues under chronic inflammation, adipose tissue exhibits interstitial fibrosis during the development of obesity. In line with this, recent evidence showed overproduction of extracellular matrix components in adipose tissue from obese animals and humans, which is implicated in systemic insulin resistance and hepatic steatosis^{6,22–24}. However, little is known about how adipose tissue fibrosis is regulated in response to overnutrition. In this study, we provide evidence suggesting that *Mincle* is a novel regulator of adipose tissue fibrosis. Although macrophages are crucial for the regulation of tissue fibrosis, macrophages can promote and regress tissue fibrosis depending on the context²⁵.

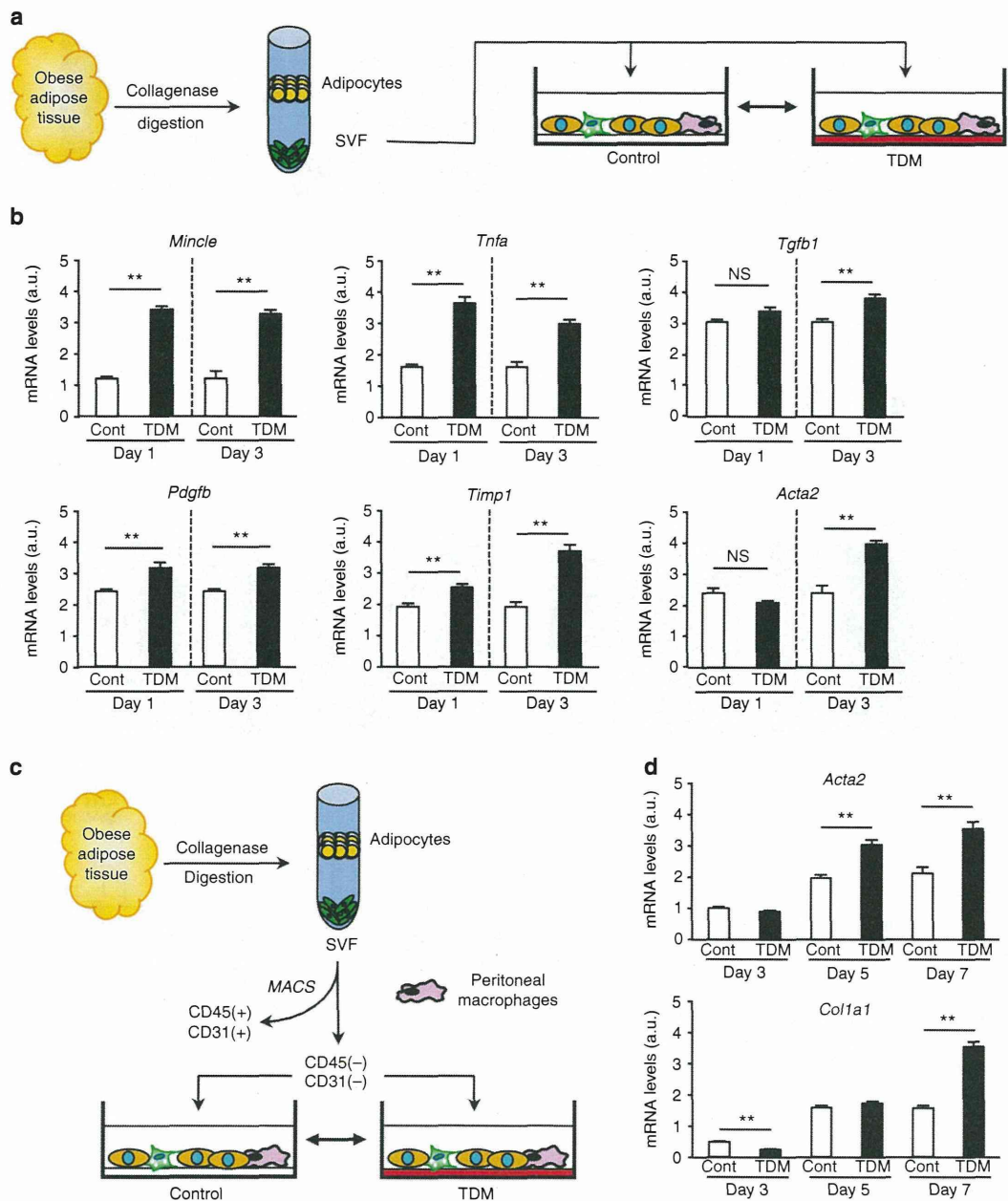


Figure 6 | Mincle-stimulated increase of myofibroblasts in SVF. (a) Illustration of the TDM-stimulated experiments using SVF. SVF prepared from epididymal fat tissue of *ob/ob* mice was stimulated with TDM for up to 3 days. (b) Effect of TDM stimulation on mRNA expression of *Mincle*, *Tnfa*, fibrosis-related genes (*Tgfb1*, *Pdgfb*, *Timp1*) and *Acta2*. Values are mean \pm s.e.m. The data are analysed by unpaired *t*-test; *n* = 4, ***P* < 0.01, NS, not significant. (c,d) Co-culture experiments of peritoneal macrophages and adipose tissue fibroblasts. (c) Illustration of the co-culture experiments using peritoneal macrophages and CD45⁺CD31⁺ cells in SVF, rich in fibroblasts, prepared from epididymal fat tissue of *ob/ob* mice using the magnetic cell sorting system (MACS). The cells were stimulated with TDM for up to 7 days. (d) Effect of TDM stimulation on mRNA expression of *Acta2* and *Col1a1* (collagen I). Values are mean \pm s.e.m. The data are analysed by unpaired *t*-test; *n* = 4, ***P* < 0.01.

Our data suggest that macrophages promote adipose tissue fibrosis through Mincle during the development of obesity.

We previously reported that a paracrine loop between adipocytes and macrophages establishes a vicious cycle that augments inflammatory changes in adipose tissue during the development of obesity⁵. CLS represents a unique structure where adipocytes and macrophages crosstalk in close proximity in obese adipose tissue *in vivo*, thereby accelerating adipose tissue inflammation. The data of this study suggest that CLS is an

important origin of fibrosis as well as inflammation in adipose tissue. This notion is supported by our recent observations that the CLS-like histological structure in the liver of nonalcoholic steatohepatitis in mice and humans, which may be involved in the fibrogenesis of the liver²⁶. Given that *Mincle* expression is localized to macrophages constituting CLS and that residual lipid droplets of dead adipocytes are scavenged by macrophages within CLS, Mincle can sense as-yet-unidentified endogenous ligands that are released as danger signals from dead adipocytes in the

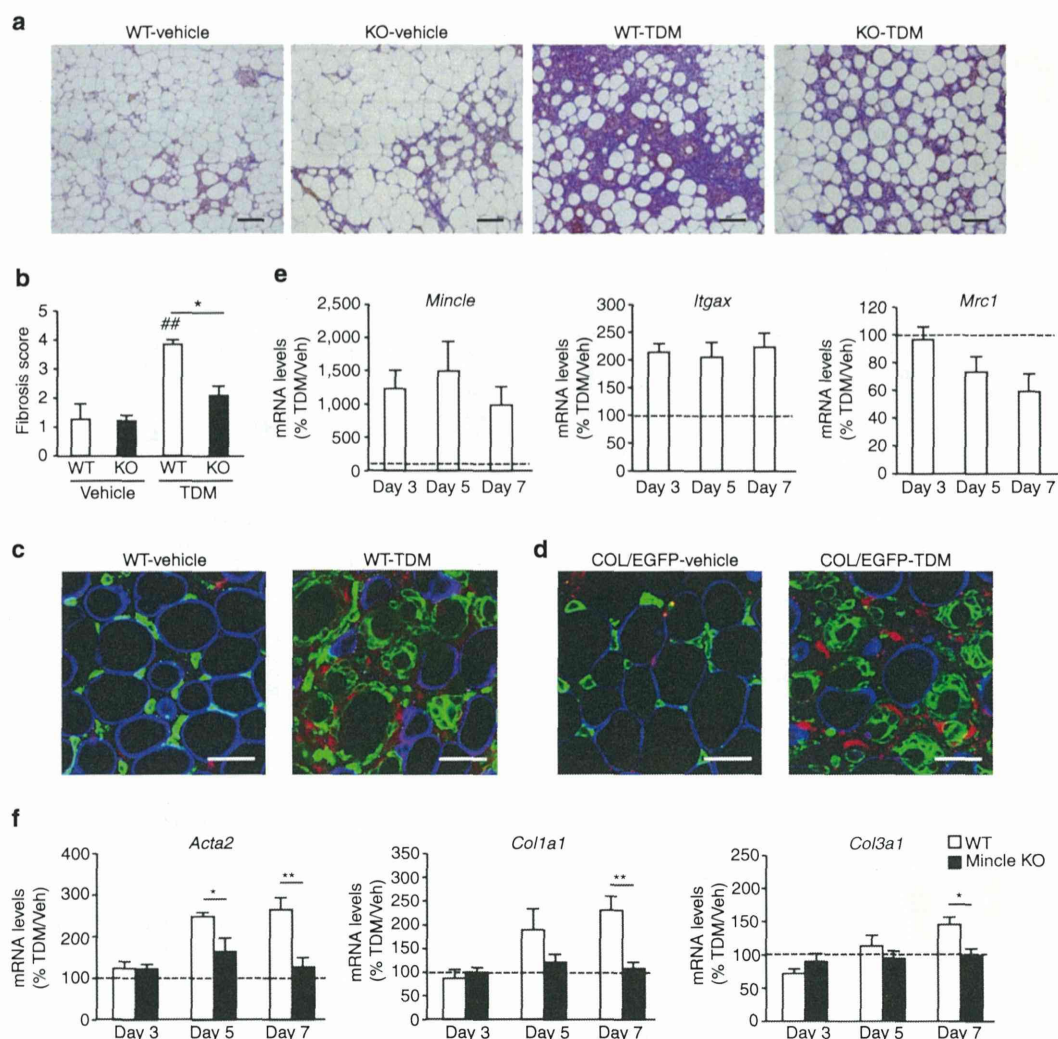


Figure 7 | Mincle-stimulated interstitial fibrosis in adipose tissue. Emulsion containing TDM or vehicle was injected into epididymal fat tissue of *Mincle* KO and wild-type mice. **(a,b)** Representative Masson's trichrome staining **(a)** and semiquantitative analysis of interstitial fibrosis **(b)** of epididymal fat tissue 7 days after injection. Original magnification, $\times 100$; Scale bar, 100 μm . Values are mean \pm s.e.m. The data are analysed by ANOVA followed by Tukey-Kramer test; $n = 4$ to 5, $^{##}P < 0.01$ versus WT-vehicle, $^{*}P < 0.05$. **(c)** Representative immunofluorescent staining of F4/80 (green), perilipin (blue) and collagen I (red) in wild-type mice treated with TDM or vehicle. Original magnification, $\times 600$; Scale bar, 50 μm . **(d)** Representative immunofluorescent staining of F4/80 (green), perilipin (blue) and EGFP (red) in COL/EGFP Tg mice treated with TDM or vehicle. Original magnification, $\times 600$; Scale bar, 50 μm . **(e,f)** Time course of mRNA expression up to 7 days after injection. mRNA expression of *Mincle*, *Itgax* and *Mrc1* in wild-type mice **(e)** and that of *Acta2*, *Col1a1* and *Col3a1* (collagen III) in *Mincle* KO and wild-type mice **(f)**. Values are mean \pm s.e.m. The data are analysed by unpaired t-test; $n = 4$ to 5, $^{*}P < 0.05$, $^{**}P < 0.01$.

interaction between adipocytes and macrophages. This is the first report to elucidate the role of *Mincle*, a pathogen sensor for pathogenic fungi and *Mycobacterium tuberculosis*, in sterile inflammation. Considering the structural and functional similarities between CLS and mycobacterial granuloma, it is interesting to compare the role of *Mincle* under those conditions. In this regard, our data indicate the critical role of *Mincle* in CLS formation in adipose tissue, which is reminiscent of the recent report by Ishikawa *et al.* that *Mincle* is essential for the TDM-induced granuloma formation in lung¹³. Moreover, CLS in adipose tissue and granuloma structure in lung are accompanied by tissue fibrosis. Taken together, it is conceivable that *Mincle* has a role in metabolic stress- as well as pathogen-induced sustained cell-to-cell communication within CLS, thereby contributing to tissue remodelling.

It is important to know how *Mincle*-expressing macrophages are involved in fibrogenesis in adipose tissue. Stimulation of *Mincle* with TDM activates Syk in macrophages to increase expression of fibrosis-related genes as well as proinflammatory cytokines. These observations are consistent with previous studies that activation of Syk can induce TGF β production in macrophages and dendritic cells^{27,28}. On the other hand, *Mincle* is selectively expressed in proinflammatory M1 macrophages and localized to some of the macrophages constituting CLS in obese adipose tissue, whereas antiinflammatory M2 macrophages, not M1 macrophages, are considered to contribute to tissue repair and remodelling. These observations led us to speculate that *Mincle*-expressing macrophages could be a novel subpopulation of adipose tissue macrophages contributing to tissue remodelling under chronic inflammatory conditions. This notion is supported

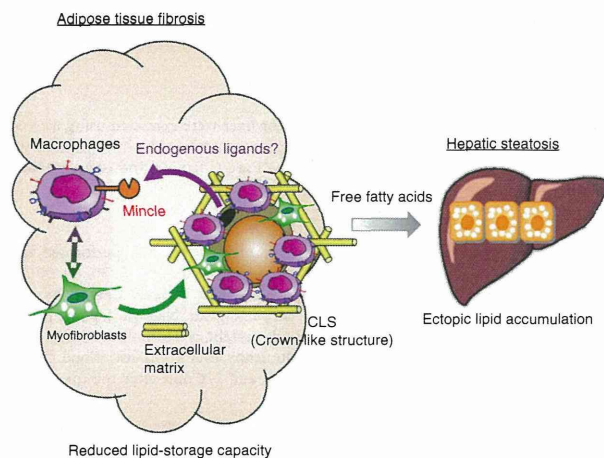


Figure 8 | Potential role of Mincle in obesity-induced adipose tissue inflammation. During the development of obesity, Mincle expression is induced in infiltrated macrophages and activated by an endogenous ligand released from dying adipocytes. Mincle is involved in macrophage aggregation to form CLS, and Mincle activation also induces expression of fibrosis-related genes thereby leading to myfibroblast formation. As a result, overproduction of ECM may limit the HFD-induced hypertrophy of adipocytes, which has a role in lipid accumulation in the liver and glucose intolerance.

by recent evidence that adipose tissue macrophages exhibit mixed phenotypes of M1 and M2 in obese humans and mice^{29–31}. Interestingly, our data show that Mincle contributes to CLS formation and fibrogenesis without affecting macrophage polarization in obesity-induced adipose tissue inflammation. Since *Mincle* expression is quite low in adipose tissue from healthy lean mice, it is conceivable that Mincle-expressing macrophages are involved in pathological tissue remodelling in adipose tissue.

Fibrogenesis is a complex process caused by a variety of cells including myfibroblasts, immune cells and parenchymal cells. In terms of adipose tissue fibrosis, it is known that expression of collagen I and III is largely derived from SVF rather than adipocytes³². However, little is known about myfibroblasts in adipose tissue. In addition, myfibroblasts are derived from different cell types such as resident fibroblasts and fibrocytes, depending upon organs and tissues²⁰. In this study, we observed increased number of α SMA-positive cells or myfibroblasts in obese adipose tissue. It is, therefore, interesting to know the origin of myfibroblasts in obese adipose tissue. In this regard, human preadipocytes are reported to be a source of ECM^{33–35}. It is also important to understand the molecular mechanisms underlying myfibroblast formation during the development of obesity. Our data suggest that Mincle stimulation in macrophages effectively increases myfibroblast formation in SVF probably through the interaction between macrophages and fibroblasts. Consistently, several studies point to the role of macrophages in promoting fibroblastic phenotype and ECM production in human preadipocytes^{33–35}. Taken together with recent observations that activation of hypoxia-inducible factor-1 in adipocytes contributes to interstitial fibrosis in adipose tissue⁸, Mincle in macrophages may link obesity-induced adipocyte damages with myfibroblast formation.

Storing excessive energy as triglyceride is a fundamental function of adipose tissue. In response to nutritional conditions, lipid metabolism in adipose tissue is tightly regulated by hormones and the sympathetic nervous system. For instance, catecholamines induce adipocyte lipolysis to supply free fatty

acids as fuel to other organs during the fasted state. On the other hand, insulin suppresses adipocyte lipolysis and facilitates lipogenesis in adipose tissue during the fed state³. In addition, accumulating evidence suggests that chronic inflammation in adipose tissue can induce ectopic lipid accumulation through several mechanisms^{3,4}. First, obesity-induced chronic inflammation causes insulin resistance in adipose tissue^{1,2}. Second, proinflammatory cytokines such as TNF α can directly induce lipolysis in adipocytes⁵. Finally, adipose tissue fibrosis may limit the expandability of adipose tissue during the development of obesity⁶. Divoux *et al.*³² reported that adipose tissue fibrosis is negatively correlated with adipocyte diameters in human adipose tissue. It is also known that adipose tissue macrophage infiltration is associated with hepatic lipid accumulation in humans³⁶. Moreover, we observed that melanocortin 4 receptor-deficient mice fed a HFD exhibit accelerated adipose tissue inflammation with interstitial fibrosis, which may contribute to excessive lipid accumulation in the liver²⁴. In line with this, *Mincle* KO mice are protected against obesity-induced adipose tissue fibrosis and ectopic lipid accumulation in the liver. We also found that serum FFA concentrations are significantly decreased in *Mincle* KO mice relative to wild-type mice. All these data support the notion that increased lipid-storage capacity of adipose tissue in *Mincle* KO mice may cause less efflux of FFA from adipose tissue to the liver. Our data highlight the role of Mincle as a novel mechanism of how chronic inflammation induces ectopic lipid accumulation in obesity.

It is important to know which organ is responsible for the ameliorated glucose tolerance in *Mincle* KO mice. In this study, *Mincle* KO mice exhibit better glucose tolerance and lower serum insulin concentrations than wild-type mice as early as 16 weeks after HFD feeding, when there is a marked reduction of hepatic steatosis in *Mincle* KO mice. Consistently, insulin sensitivity is significantly increased in the liver and tends to be ameliorated in adipose tissue and skeletal muscle as well as in *Mincle* KO mice relative to wild-type mice. These observations support the notion that activation of Mincle in adipose tissue triggers ectopic lipid accumulation and insulin resistance in the liver, thereby inducing systemic glucose intolerance. On the other hand, we do not exclude the possibility that Mincle in non-adipose tissues has a role in obesity-induced ectopic lipid accumulation and insulin resistance, since obesity also induces *Mincle* expression in liver to a lesser extent than adipose tissue. Further studies are required to elucidate the molecular mechanisms underlying Mincle-mediated glucose intolerance in obesity.

On the basis of our observations, we hypothesize a role of Mincle in adipose tissue inflammation in obesity as follows (Fig. 8). During the development of obesity, Mincle expression is induced mainly through TLR4 in infiltrated macrophages as we previously reported¹⁸. Activated by an endogenous ligand released from dying adipocytes, Mincle is involved in macrophage aggregation to form CLS, where there is a sustained interaction between adipocytes and macrophages. Mincle activation also induces expression of fibrosis-related genes through Syk, thereby leading to myfibroblast formation possibly through intercellular communication between macrophages and fibroblasts. As a result, overproduction of ECM may limit the HFD-induced hypertrophy of adipocytes, which has a role in lipid accumulation in the liver and glucose intolerance.

In summary, we demonstrated in this study that Mincle has a critical role in HFD-induced CLS formation and adipose tissue fibrosis, which may reduce lipid-storage capacity in adipose tissue and enhance ectopic lipid accumulation. Our data also suggest that Mincle in macrophages would be a novel therapeutic target to prevent or treat obesity-induced adipose tissue inflammation and metabolic derangement.

Methods

Reagents. All reagents were purchased from Sigma-Aldrich (St Louis, MO) or Nacalai Tesque (Kyoto, Japan) unless otherwise noted.

Animals. The *Mincle* KO mice and enhanced green fluorescence protein (*Egfp*) Tg mice on the C57BL/6J genetic background were kindly provided by Drs Shizuo Akira and Masaru Okabe (Osaka University)^{16,37}, respectively. We crossed these mice to generate the *Mincle* KO-*Egfp* Tg mice for the BMT experiments. Eight-week-old C57BL/6J-*ob/ob* and wild-type mice were purchased from Japan SLC (Shizuoka, Japan). They were maintained in a temperature-, humidity- and light-controlled room (12 h light/dark cycles), allowed free access to water and standard chow (CE-2; 343.1 kcal per 100 g, 12.6% energy as fat; CLEA Japan, Tokyo, Japan). Ten-week-old animals were fed either an SD (CE-2) or HFD (D12492; 556 kcal per 100 g, 60% energy as fat; Research Diets, New Brunswick, NJ) for 8, 16 and 50 weeks. The COL-EGFP Tg mice on the C57BL/6J background, which express EGFP exclusively in collagen I-producing cells, were used to detect myofibroblasts³⁸. All animal experiments were approved by the Institutional Animal Care and Use Committee of Tokyo Medical and Dental University (No.2011-207C, No.0140016A). We used male 9–11-week-old mice with a C57BL/6J background in all experiments in the present study unless otherwise noted.

Histological analysis. The epididymal fat tissue and liver were fixed with neutral-buffered formalin and embedded in paraffin. Two-micrometre thick sections were stained with hematoxylin and eosin, Masson's Trichrome, or Sirius red. For the measurement of adipocyte cell size, more than 200 cells were counted per each section using an image analysis software (WinRoof; Mitani, Tokyo, Japan). Fibrosis and α SMA-positive area were measured by an image analysis software (Dynamic Cell Count; Keyence, Osaka, Japan). The presence of F4/80-positive macrophages in epididymal fat tissue was detected immunohistochemically using the rat monoclonal anti-mouse F4/80 antibody kindly provided by Dr Motohiro Takeya (Kumamoto University)^{39,40}. The number of F4/80-positive cells was counted in more than 10 mm² area of each section and expressed as the mean number per mm². The CLS density was obtained by counting the total numbers of CLS and adipocytes in each section, which was expressed as CLS number per 10,000 adipocytes⁴¹. Antibodies used in this study for immunohistochemistry are listed in Supplementary Table 2. To evaluate the TDM-induced adipose tissue fibrosis, the sections were graded semiquantitatively (scores 0 to 4) according to the Masson's trichrome-positive area (0 = none, 1 = weak, 2 = mild, 3 = moderate, 4 = severe). The representative histological images for the respective score values were shown in Supplementary Fig. 9. The quantitative histological analysis was performed by three investigators who had no knowledge of the origin of the slides.

In situ hybridization. *In situ* hybridization for *Mincle* mRNA was performed as reported⁴². Paraffin-embedded tissue blocks from epididymal fat tissue were sectioned at 8 μ m. The sections were fixed with 4% paraformaldehyde for 15 min, treated with 8 μ g ml⁻¹ proteinase K for 30 min at 37 °C, re-fixed with 4% paraformaldehyde and then acetylated with 0.25% acetic anhydride for 10 min. Hybridization was performed with probes at concentrations of 300 ng ml⁻¹ at 60 °C for 16 h. After hybridization, the sections were washed in 5 \times saline sodium citrate (SSC) at 60 °C for 20 min and then in 50% formamide and 2 \times SSC at 60 °C for 20 min, followed by treatment with 50 μ g ml⁻¹ RNaseA for 30 min at 37 °C. After the sections were further washed several times with 2 \times SSC and 0.2 \times SSC, they were incubated with anti-DIG AP conjugate (Roche) for 1 h at room temperature. After washing twice, colouring reactions were performed with NBT/BCIP solution (Roche) overnight. Several sections were double stained with a macrophage marker, Iba1.

Flow cytometric analyses. Flow cytometric analyses of SVF were performed as described^{43,44}. In brief, the epididymal fat tissue was collected and cut into small pieces and incubated for 20 min in collagenase solution (2 mg ml⁻¹ of collagenase type 2 (Worthington, Lakewood, NJ)) with gentle shaking. After filtering through a 180- μ m mesh, we centrifuged it and resuspended in phosphate-buffered saline (PBS). We washed the dissociated SVF twice with PBS, incubated them for 10 min in erythrocyte-lysing buffer and filtered it through a 70- μ m mesh. Cells were sorted using FACSAriaII (BD Biosciences, San Jose, CA) and used for mRNA expression analysis. *Mincle*-expressing cells were analysed using FACSCantoII (BD Biosciences) and FlowJo 7.2.2. software (Tomy Digital Biology, Tokyo, Japan). *Mincle*-expressing cells were identified by anti-*Mincle* antibody (clone 4A9; MBL, Nagoya, Japan) labelled with Lightning-Link Atto-488 (Innova Biosciences, Cambridge, UK). Other antibodies used in flow cytometric analyses were listed in Supplementary Table 3.

Confocal microscopic analysis. For confocal microscopic analysis, isolated tissue pieces were fixed in 4% formaldehyde and permeabilized with 0.5% Triton X-100. The specimens were then blocked with 1% BSA and incubated with a pair of primary antibodies and then with the respective secondary antibodies. The stainings were examined by using the FluoView FV10i confocal microscope system (Olympus, Tokyo, Japan).

Collagen content in adipose tissue. Total collagen content in adipose tissue was measured using a commercially available kit (The QuickZyme total collagen assay; QuickZyme Biosciences, Leiden, Netherlands).

Triglyceride content in liver. Total lipids in the liver were extracted using ice-cold chloroform and methanol, 2:1 (v/v). Triglyceride content in the liver content was measured using an enzymatic assay kit (Wako Pure Chemical Industries, Osaka, Japan).

Glucose and insulin tolerance tests. Glucose tolerance test was performed after an 18-h fast. Blood glucose concentrations were measured at 0, 15, 30, 60, 90 and 120 min after intraperitoneal injection of glucose (2 g kg⁻¹ body weight) by a blood glucose test meter (Glutest PRO R; Sanwa-Kagaku, Nagoya, Japan). For insulin tolerance test, insulin (0.5 U kg⁻¹ body weight of Humulin R-Insulin; Eli Lilly, Indianapolis, IN) was injected intraperitoneally after a 1-h fast. Blood glucose concentrations were measured 0, 15, 30, 60, 90 and 120 min after the injection.

Western blotting of Akt. Western blotting was performed as described⁴⁵. In brief, mice with food deprivation for 16 h were injected with insulin (0.5 U kg⁻¹ body weight of Humulin R-Insulin; Eli Lilly) or PBS via the postcaval vein. Liver, soleus muscle and epididymal fat tissue were removed 1, 2 and 3 min after the injection, respectively. Immunoblotting was performed using anti-phospho-Akt (Thr308) antibody (Cell Signaling Technology, Danvers, MA) and anti-Akt antibody (Santa Cruz Biotechnology, Santa Cruz, CA). Immunoblot images were quantified using ImageQuant LAS 4000 mini (Fujifilm, Tokyo, Japan). Representative uncropped blots are shown in Supplementary Fig. 10.

Serum analysis. Serum FFA and ALT, and insulin concentrations were measured using a standard enzymatic assay or a commercially available enzyme-linked immunosorbent assay kit.

TDM stimulation. For stimulation of thioglycollate-elicited peritoneal macrophages or SVF from epididymal fat tissue of *ob/ob* mice, TDM dissolved in chloroform at 1 mg ml⁻¹ were diluted in isopropanol and added on 12- or 48-well culture plates (5 or 1.25 μ g of TDM per well, respectively), followed by evaporation of the solvent as described^{13,46}. In some experiments, peritoneal macrophages were co-cultured with adipose tissue fibroblasts (CD45⁻CD31⁻ cells prepared from SVF of *ob/ob* mice using the magnetic cell sorting system (MACS; Miltenyi Biotec, Auburn, CA)). For *in vivo* experiments, the emulsion containing TDM (10 μ g; ref. 13) was directly injected into epididymal fat tissue. Three, five and seven days after the injection, the epididymal fat tissue was collected and subjected to gene expression analysis and Masson's trichrome and immunofluorescent stainings.

Quantitative real-time PCR. Quantitative real-time PCR was performed as described¹⁸. In brief, total RNA was extracted from the tissues or cultured cells using Sepasol reagent and 10 ng of cDNA was used for real-time PCR amplification with SYBR GREEN detection protocol in a thermal cycler (StepOne Plus, Applied Biosystems, Foster City, CA). Primers used in this study are listed in Supplementary Table 4. Data were normalized to the *36B4* levels, and analysed using the comparative CT method.

Microarray analysis. Microarray analysis was performed using Affymetrix GeneChip Mouse Genome 430 2.0 Arrays according to the manufacturer's instructions. Normalization of gene expression data was processed using the Affymetrix Microarray Analysis Suite 5.0 (MAS5) algorithms. Differentially expressed genes were selected with fold change and *P* value (fold change > 2, *P* < 0.01). Pathway and gene ontology analyses were performed using the Reactome functional protein interaction database (<http://www.reactome.org/>).

BMT experiments. BMT was performed as described³⁹. In brief, bone marrow cells obtained from *Mincle* KO-*Egfp* Tg mice and *Egfp* Tg mice were washed three times with cold PBS and injected intravenously (1.8×10^6 cells) into 7.5 Gy irradiated 8-week-old male wild-type recipient mice. After 4 weeks, the substitution rate of bone marrow cells was determined by counting EGFP-positive cells in the peripheral blood and then the mice were fed a HFD for 16 weeks.

Statistical analysis. Data are presented as the mean \pm s.e.m., and *P* < 0.05 and *P* < 0.01 were considered statistically significant. Statistical analysis was performed using analysis of variance followed by Tukey–Kramer test. Unpaired *t*-test was used to compare two groups. In the GTT and ITT data, the entire curves were analysed using repeated-measures analysis of variance adjusted with degrees of freedom by Huynh and Feldt if the Mauchly's sphericity test is significant (*P* < 0.05).

References

- Hotamisligil, G. S. Inflammation and metabolic disorders. *Nature* **444**, 860–867 (2006).
- Olefsky, J. M. & Glass, C. K. Macrophages, inflammation, and insulin resistance. *Annu. Rev. Physiol.* **72**, 219–246 (2010).
- Suganami, T., Tanaka, M. & Ogawa, Y. Adipose tissue inflammation and ectopic lipid accumulation. *Endocr. J.* **59**, 849–857 (2012).
- Sun, K., Kusminski, C. M. & Scherer, P. E. Adipose tissue remodeling and obesity. *J. Clin. Invest.* **121**, 2094–2101 (2011).
- Suganami, T., Nishida, J. & Ogawa, Y. A paracrine loop between adipocytes and macrophages aggravates inflammatory changes: role of free fatty acids and tumor necrosis factor alpha. *Arterioscler. Thromb. Vasc. Biol.* **25**, 2062–2068 (2005).
- Khan, T. *et al.* Metabolic dysregulation and adipose tissue fibrosis: role of collagen VI. *Mol. Cell. Biol.* **29**, 1575–1591 (2009).
- Jonker, J. W. *et al.* A PPAR γ -FGF1 axis is required for adaptive adipose remodelling and metabolic homeostasis. *Nature* **485**, 391–394 (2012).
- Sun, K., Halberg, N., Khan, M., Magalang, U. J. & Scherer, P. E. Selective inhibition of hypoxia-inducible factor 1 α ameliorates adipose tissue dysfunction. *Mol. Cell. Biol.* **33**, 904–917 (2013).
- Cinti, S. *et al.* Adipocyte death defines macrophage localization and function in adipose tissue of obese mice and humans. *J. Lipid. Res.* **46**, 2347–2355 (2005).
- Lumeng, C. N., Bodzin, J. L. & Saltiel, A. R. Obesity induces a phenotypic switch in adipose tissue macrophage polarization. *J. Clin. Invest.* **117**, 175–184 (2007).
- Apovian, C. M. *et al.* Adipose macrophage infiltration is associated with insulin resistance and vascular endothelial dysfunction in obese subjects. *Arterioscler. Thromb. Vasc. Biol.* **28**, 1654–1659 (2008).
- Bremer, A. A., Devaraj, S., Afify, A. & Jialal, I. Adipose tissue dysregulation in patients with metabolic syndrome. *J. Clin. Endocrinol. Metab.* **96**, E1782–E1788 (2011).
- Ishikawa, E. *et al.* Direct recognition of the mycobacterial glycolipid, trehalose dimycolate, by C-type lectin Mincle. *J. Exp. Med.* **206**, 2879–2888 (2009).
- Schoenen, H. *et al.* Cutting edge: Mincle is essential for recognition and adjuvanticity of the mycobacterial cord factor and its synthetic analog trehalose-dibehenate. *J. Immunol.* **184**, 2756–2760 (2010).
- Wells, C. A. *et al.* The macrophage-inducible C-type lectin, mincle, is an essential component of the innate immune response to *Candida albicans*. *J. Immunol.* **180**, 7404–7413 (2008).
- Yamasaki, S. *et al.* C-type lectin Mincle is an activating receptor for pathogenic fungus, *Malassezia*. *Proc. Natl Acad. Sci. USA* **106**, 1897–1902 (2009).
- Matsumoto, M. *et al.* A novel LPS-inducible C-type lectin is a transcriptional target of NF- κ B in macrophages. *J. Immunol.* **163**, 5039–5048 (1999).
- Ichioika, M. *et al.* Increased expression of macrophage-inducible C-type lectin in adipose tissue of obese mice and humans. *Diabetes* **60**, 819–826 (2011).
- Yamasaki, S. *et al.* Mincle is an ITAM-coupled activating receptor that senses damaged cells. *Nat. Immunol.* **9**, 1179–1188 (2008).
- Wynn, T. A. & Ramalingam, T. R. Mechanisms of fibrosis: therapeutic translation for fibrotic disease. *Nat. Med.* **18**, 1028–1040 (2012).
- Hinz, B. *et al.* The myofibroblast: one function, multiple origins. *Am. J. Pathol.* **170**, 1807–1816 (2007).
- Liu, J. *et al.* Genetic deficiency and pharmacological stabilization of mast cells reduce diet-induced obesity and diabetes in mice. *Nat. Med.* **15**, 940–945 (2009).
- Mutch, D. M. *et al.* Needle and surgical biopsy techniques differentially affect adipose tissue gene expression profiles. *Am. J. Clin. Nutr.* **89**, 51–57 (2009).
- Itoh, M. *et al.* Melanocortin 4 receptor-deficient mice as a novel mouse model of nonalcoholic steatohepatitis. *Am. J. Pathol.* **179**, 2454–2463 (2011).
- Duffield, J. S. *et al.* Selective depletion of macrophages reveals distinct, opposing roles during liver injury and repair. *J. Clin. Invest.* **115**, 56–65 (2005).
- Itoh, M. *et al.* Hepatic crown-like structure: a unique histological feature in non-alcoholic steatohepatitis in mice and humans. *PLoS ONE* **8**, e82163 (2013).
- Lipinski, T. *et al.* Enhanced immunogenicity of a tricomponent mannan tetanus toxoid conjugate vaccine targeted to dendritic cells via Dectin-1 by incorporating β -glucan. *J. Immunol.* **190**, 4116–4128 (2013).
- Takamiya, R., Ohtsubo, K., Takamatsu, S., Taniguchi, N. & Angata, T. The interaction between Siglec-15 and tumor-associated sialyl-Tn antigen enhances TGF- β secretion from monocytes/macrophages through the DAP12-Syk pathway. *Glycobiology* **23**, 178–187 (2013).
- Shaul, M. E., Bennett, G., Strissel, K. J., Greenberg, A. S. & Obin, M. S. Dynamic, M2-like remodeling phenotypes of CD11c $^{+}$ adipose tissue macrophages during high-fat diet–induced obesity in mice. *Diabetes* **59**, 1171–1181 (2010).
- Wentworth, J. M. *et al.* Pro-inflammatory CD11c $^{+}$ CD206 $^{+}$ adipose tissue macrophages are associated with insulin resistance in human obesity. *Diabetes* **59**, 1648–1656 (2010).
- Zeyda, M. *et al.* Human adipose tissue macrophages are of an anti-inflammatory phenotype but capable of excessive pro-inflammatory mediator production. *Int. J. Obes. (Lond)* **31**, 1420–1428 (2007).
- Divoux, A. *et al.* Fibrosis in human adipose tissue: composition, distribution, and link with lipid metabolism and fat mass loss. *Diabetes* **59**, 2817–2825 (2010).
- Bourlier, V. *et al.* TGF β family members are key mediators in the induction of myofibroblast phenotype of human adipose tissue progenitor cells by macrophages. *PLoS ONE* **7**, e31274 (2012).
- Gagnon, A., Yarmo, M. N., Landry, A. & Sorisky, A. Macrophages alter the differentiation-dependent decreases in fibronectin and collagen I/III protein levels in human preadipocytes. *Lipids* **47**, 873–880 (2012).
- Keophiphath, M. *et al.* Macrophage-secreted factors promote a profibrotic phenotype in human preadipocytes. *Mol. Endocrinol.* **23**, 11–24 (2009).
- Lê, K. A. *et al.* Subcutaneous adipose tissue macrophage infiltration is associated with hepatic and visceral fat deposition, hyperinsulinemia, and stimulation of NF- κ B stress pathway. *Diabetes* **60**, 2802–2809 (2011).
- Okabe, M., Ikawa, M., Kominami, K., Nakanishi, T. & Nishimune, Y. ‘Green mice’ as a source of ubiquitous green cells. *FEBS Lett.* **407**, 313–319 (1997).
- Higashiyama, R. *et al.* Negligible contribution of bone marrow-derived cells to collagen production during hepatic fibrogenesis in mice. *Gastroenterology* **137**, 1459–1466 (2009).
- Ito, A. *et al.* Role of CC chemokine receptor 2 in bone marrow cells in the recruitment of macrophages into obese adipose tissue. *J. Biol. Chem.* **283**, 35715–35723 (2008).
- Kitagawa, K. *et al.* Blockade of CCR2 ameliorates progressive fibrosis in kidney. *Am. J. Pathol.* **165**, 237–246 (2004).
- Murano, I. *et al.* Dead adipocytes, detected as crown-like structures, are prevalent in visceral fat depots of genetically obese mice. *J. Lipid. Res.* **49**, 1562–1568 (2008).
- Miyake, Y. *et al.* C-type lectin MCL is an Fc γ -coupled receptor that mediates the adjuvanticity of mycobacterial cord factor. *Immunity* **38**, 1050–1062 (2013).
- Tanaka, M. *et al.* Role of central leptin signaling in the starvation-induced alteration of B-cell development. *J. Neurosci.* **31**, 8373–8380 (2011).
- Nishimura, S. *et al.* Adipose natural regulatory B cells negatively control adipose tissue inflammation. *Cell Metab.* **18**, 759–766 (2013).
- Murano, K. *et al.* Histidine augments the suppression of hepatic glucose production by central insulin action. *Diabetes* **62**, 2266–2277 (2013).
- Ozeki, Y. *et al.* Macrophage scavenger receptor down-regulates mycobacterial cord factor-induced proinflammatory cytokine production by alveolar and hepatic macrophages. *Microb. Pathog.* **40**, 171–176 (2006).

Acknowledgements

We thank Drs Shizuo Akira and Masaru Okabe, Osaka University, for the generous gift of *Mincle* KO mice and *Egfp* Tg mice, respectively, and Dr Takahisa Nakamura, Cincinnati Children's Hospital Medical Center, for critical reading of the manuscript. This work was supported in part by Grants-in-Aid for Scientific Research from the Ministry of Education, Culture, Sports, Science and Technology of Japan, the Ministry of Health, Labour and Welfare of Japan, and Japan Science and Technology Agency, PRESTO. This work was also supported by research grants from Takeda Medical Research Foundation, The Tokyo Biochemical Research Foundation, Astellas Foundation for Research on Metabolic Disorders, The Mochida Memorial Foundation for Medical and Pharmaceutical Research and The Ichiro Kanehara Foundation.

Author contributions

M.T. and K.I. researched the data, contributed to the discussion and wrote the manuscript. C.K., K.O., I.S., M.H., K.K. and H.I. researched the data. T.M. contributed to cDNA microarray analysis. S.N., I.M., Y.I. and S.A. contributed to the histological analysis. S.Y. contributed to the discussion. T.S. and Y.O. contributed to the discussion and wrote, reviewed and edited the manuscript.

Additional information

Accession codes: Microarray data have been deposited in the NCBI Gene Expression Omnibus (GEO) under accession code GSE52338.

Supplementary Information accompanies this paper at <http://www.nature.com/naturecommunications>

Competing financial interests: The authors declare no competing financial interests.

Reprints and permission information is available online at <http://npg.nature.com/reprintsandpermissions/>

How to cite this article: Tanaka, M. *et al.* Macrophage-inducible C-type lectin underlies obesity-induced adipose tissue fibrosis. *Nat. Commun.* **5**:4982 doi: 10.1038/ncomms5982 (2014).

